

# Braking protons at the EIC: from invisible meson decay to new physics searches

Reuven Balkin,<sup>1</sup> Ta’el Coren,<sup>2</sup> Alexander Jentsch,<sup>3</sup> Hongkai Liu,<sup>3</sup> Maksym Ovchynnikov,<sup>4</sup> Yotam Soreq,<sup>2, 4</sup> and Sokratis Trifinopoulos<sup>5, 4, 6</sup>

<sup>1</sup>*Department of Physics, University of California Santa Cruz and Santa Cruz Institute for Particle Physics, 1156 High St., Santa Cruz, CA 95064, USA*

<sup>2</sup>*Physics Department, Technion - Israel Institute of Technology, Haifa 3200003, Israel*

<sup>3</sup>*Department of Physics, Brookhaven National Laboratory, Upton, NY 11973, USA*

<sup>4</sup>*Theoretical Physics Department, CERN, 1211 Geneva 23, Switzerland*

<sup>5</sup>*Center for Theoretical Physics – a Leinweber Institute, Massachusetts Institute of Technology, Cambridge, MA 02139, USA*

<sup>6</sup>*Physik-Institut, Universität Zürich, 8057 Zürich, Switzerland*

We investigate the sensitivity of the Electron-Ion Collider (EIC) to invisible final states in coherent exclusive electroproduction. The characteristic signal is a forward proton with reduced energy and little additional detector activity. Using the excellent particle detection capabilities and kinematics reconstruction at the EIC, we argue that backgrounds can be strongly suppressed. While our analysis applies to various states, we specifically focus on pseudoscalar particles: (i) neutral mesons ( $\pi^0, \eta^{(\prime)}$ ), whose invisible Standard Model decays are extremely suppressed, and (ii) gluon-coupled axion-like particles (ALPs) decaying invisibly to a dark sector. Depending on the meson species and the achievable background rejection, the EIC could strengthen existing bounds on invisible decays of pseudoscalar mesons by up to four orders of magnitude, probing branching ratios as small as  $\text{BR}(\eta^{(\prime)} \rightarrow \text{inv}) \sim 10^{-8}$ . In addition, the EIC would directly probe invisibly decaying ALPs with the couplings up to  $f_a \sim 10^5$  GeV and masses in the range 0.1–2 GeV.

**Introduction.** The upcoming Electron-Ion Collider (EIC) [1, 2], to be built at Brookhaven National Laboratory, will collide electrons of up to 18 GeV with protons of up to 275 GeV (or nuclei from deuterons to Uranium), reaching annual integrated luminosities  $\mathcal{L}_{\text{int}} = 100 \text{ fb}^{-1}$ . Its physics program is primarily devoted to unraveling the partonic structure of nucleons and nuclei, but its kinematic reach and detector capabilities also make it a powerful laboratory for searches for rare and exotic processes, offering sensitive probes of physics beyond the Standard Model (SM) [3–25].

A distinctive feature of the EIC relevant for this work is its far-forward detector (FFD) system [26, 27], which covers the forward-going protons ( $\eta_{p'} > 4.5$ ) up to very large pseudorapidities. This provides capabilities for exploring various signatures involving such protons. Coherent exclusive electroproduction with the *invisible* final state  $X$ ,

$$p(p_p) + e^-(p_e) \rightarrow p(p_{p'}) + e^-(p_{e'}) + X(p_X), \quad (1)$$

stands out as an especially promising target.

We consider two cases for the particle  $X$ . *Firstly*, we take it to denote the SM neutral mesons  $\{\pi^0, \eta, \eta', \rho^0, \omega, \dots\}$ . Such mesons are short-lived and decay visibly within the SM [28]. However, invisible decay channels arise naturally in many extensions involving hidden sectors [29–36], including scenarios with decays to sterile neutrinos [37] or to particles that can accommodate the dark matter relic density [38–42]. *Secondly*, we identify  $X$  with a new, beyond-the-SM particle that can be copiously produced in  $e p$  collisions and evades detection as well. For example, it could be a new spin-0 or spin-1 particle, which is coupled to hadrons and is either long-lived or decays into a dark sector.

If such invisible channels exist, the process in Eq. (1)

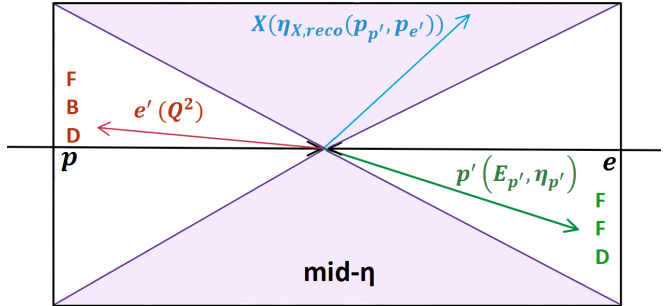


FIG. 1. An illustration of the EIC missing-proton-energy (MPE) search in  $e + p \rightarrow e' + p' + X$  events. Without relying on reconstructing  $X$ , its pseudorapidity  $\eta_X$  is indirectly extracted ( $\eta_{X,\text{reco}}(p_{e'}, p_{p'})$ ) from the kinematics of outgoing states  $e'$ ,  $p'$ . The latter are reconstructed by the far-forward (FFD) and far-backward (FBD) detectors if the event’s  $Q^2, E_{p'}, \eta_{p'}$  fall under detectability ranges (see Tbl. I). Events with  $\eta_X < 4$  are within the *fully* detector-instrumented region; thus, visible  $X$  can be vetoed, leaving only invisible states. See text for details.

would lead to a significant loss of proton energy with no accompanying detector activity. Current limits on invisible branching ratios of SM mesons [43, 44] leave ample room for the EIC to achieve major improvements. In this work, we propose a *missing-proton-energy* (MPE) search strategy at the EIC, see Fig. 1, based on the efficient tagging of the forward proton by the FFD and on reconstructing the full event kinematics by additionally seeing the scattered electron. This provides significant background suppression and enables broad parameter space exploration. The uniqueness of the MPE over other missing energy searches at the EIC, such as the

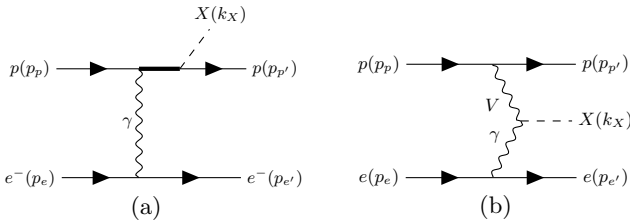


FIG. 2. Feynman diagrams for  $ep \rightarrow epX$  with  $X = \pi^0, \eta^{(\prime)}$ , (a): proton bremsstrahlung-type emission of  $X$  via the final state radiation (the similar initial-state-radiation diagram is not shown), (b)  $\gamma$ - $V$  fusion production of  $X$ .

missing-electron-energy search in Ref. [22], is its sensitivity to  $X$  particles with hadronic interactions. This has important consequences both for the rare invisible meson decays and BSM searches.

Regarding  $X$ , we focus for concreteness on the pseudoscalar case (see Fig. 2), with mesons  $P = \{\pi^0, \eta, \eta'\}$  and the axion-like particles (ALPs)  $a$  that couple to the SM primarily via gluons, see Eq. (3) below. ALPs are well-motivated extensions of the SM, appearing as generalizations of the QCD axion [45–48], originally introduced as a solution to the strong CP problem and extensively studied as a dark matter candidate [49–53] and as a portal to hidden sectors [54–59].

Our calculation of the coherent electroproduction cross sections for pseudoscalar states is based on Ref. [60] and can also be validated by a data-driven method. Our results, summarized in Tbl. II and Fig. 3, show that the same experimental analysis can both improve the sensitivity for neutral meson invisible decays by several orders of magnitude and probe previously unexplored ALP parameter space. Supplemental Material (SuM) provides details on the kinematics of the signal processes, as well as on simulations and background estimates.

**Detector description.** The first experiment being constructed at the EIC is the Electron-Proton/Ion Collider (ePIC) detector. It contains elements of high-resolution tracking, electromagnetic and hadronic calorimetry, Cherenkov and time-of-flight particle identification, and beam-line detectors for tagging exclusive processes [61]. The EIC may operate with a broad range of the incoming proton and electron energies  $E_p = 41, 100 - 275$  GeV,  $E_e = 5 - 18$  GeV. In addition to ePIC, there is a growing interest in building a second detector at the EIC. It would be complementary to ePIC for discovery confirmation between two independent experiments, but with potentially different technologies to additionally focus on other measurements [62, 63].

Considering the scattering process in Eq. (1), we use the electron transferred momentum  $Q^2 \equiv -(p_e - p_{e'})^2$ , as well as the outgoing proton's energy  $E_{p'}$  and pseudorapidity  $\eta_{p'}$  to characterize the measured electron  $e'$  and proton  $p'$ . In ePIC, there are two  $Q^2$  windows where  $e'$  may be reconstructed with a standard tracking and calorimetry technique, providing its energy-momentum

Selection	Baseline	Optimal
$E_p, E_e$	$(100, 10)$ GeV	$(41, 5)$ GeV
$p', X$	$\eta_{p'} > 4.5, 0.5 < E_{p'}/E_p < 0.9, \eta_X < 4$	—
$e'$	$10^{-3} \text{ GeV}^2 < Q^2 < 0.1 \text{ GeV}^2$	—
Bkg	0 (bg,free), Eq. (2) (bg,cons)	0

TABLE I. Two kinematics selection criteria of the outgoing proton  $p'$ , electron  $e'$ , and  $X$  from the process of Eq. (1), and backgrounds assumptions.

measurement:  $10^{-3} < Q^2 < 0.1 \text{ GeV}^2$  and  $Q^2 > 1 \text{ GeV}^2$ . We restrict our attention to the first domain, which is populated by the majority of signal events in Eq. (1), see SuM for details. For this domain,  $e'$  typically has pseudorapidity  $\eta_{e'} < -4$  and may be reconstructed by the Far-Backward Detector (FBD).

On the proton side, the FFD system covers the proton-going direction to large pseudorapidities, with dedicated off-momentum proton tagging. In the current ePIC layout, protons with a momentum greater than 40% of the beam momentum can be reconstructed with  $\simeq 100\%$  efficiency for  $\eta_{p'} > 4.5$  in the instrumented sections, with some areas uncovered due to the presence of necessary machine components (e.g., beam pipes, magnet components), or proximity to the actual beam itself (e.g. for protons with very small angles). The latter region could be extended with the second interaction region proposed in Ref. [64].

Besides the recoil proton and electron, all other visible particles are reliably reconstructed by the mid- $\eta$  detector for  $|\eta| < 4$ . Although reconstruction at larger pseudorapidities is in principle possible, it is significantly affected by instrumentation limitations in the forward region, leading to reduced and non-uniform acceptance; these effects are discussed in the SuM and are not considered in the main search.

The EIC lepton-hadron environment is effectively free of pileup, so bunch-crossing timing and vertex association can be used straightforwardly for object-level reconstruction. For the electron in the relevant  $Q^2$  domain, backward tracking and electromagnetic calorimeter (ECAL) measure  $E_{e'}$ ,  $\theta_{e'}$ , and  $\phi_{e'}$  with precision  $\delta E_{e'}/E_{e'} = (1\%)/\sqrt{E_{e'}} \oplus 1\%$  and  $\delta[\tan \theta_{e'}]/\tan \theta_{e'} \sim 2\%$  (similar for  $\phi_{e'}$ ), where  $\delta[x]$  denotes the combined uncertainty on  $x$ . The forward proton is reconstructed via transport through the machine optics to yield  $(E'_{p'}, \eta_{p'})$  with  $\delta[p_{T,p'}]/p_{T,p'} \sim 5\%$  for a transverse momentum  $p_{T,p'} \sim 1 \text{ GeV}$  and  $\delta[p_{p'}]/p_{p'} \sim 3\%$ . Reconstructing  $e', p'$ , it is possible to indirectly reconstruct  $X$  or its decay products even if they are not detected (which covers both the signal and background cases); in particular, the reconstructed pseudorapidity  $\eta_{X,\text{reco}}(p_{e'}, p_{p'})$  reproduces the true  $\eta_X$  with a relative resolution of about 5%.

**Background categories and proposed selection.** SM channels with neutrinos in the final state, for example, decays of intermediate resonances into  $\nu\bar{\nu}$ , give an *irreducible* contribution to the MPE events. Their cross sections are suppressed by the Fermi coupling and by

phase space, and the expected yield over a full EIC run is well below one event; quantitative estimates are given in the SuM. The dominant concern is therefore *reducible* background from processes that may mimic an invisible signature.

We group these backgrounds into two main classes:

1. *Beam-related and instrumental*: accidental overlaps (e.g., beam-gas collisions), particles traversing small uninstrumented gaps in fiducial acceptance, or rare reconstruction failures.
2. *Leakage of visible states*: events of the type Eq. (1) in which the state  $X$  is visible but not detected. This can occur either when  $X$  (or its decay products) is produced at large pseudorapidity,  $\eta_X \gtrsim 4$ , where the detector coverage is incomplete as described above, or when  $X$  lies in the fully instrumented region  $\eta_X < 4$  but its decay products fail to be reconstructed because of finite detection efficiency.

A reliable determination of the first class of background requires detector runs; here we only outline general handles such as tight timing and vertex matching, global vetoes on additional activity in central and forward detectors, and the exclusion of events with elastic-like kinematics, for example  $|\mathbf{p}_{T,e'}| \simeq |\mathbf{p}_{T,p'}|$ . Further discussion is provided in the SuM.

Regarding the second class, we construct a selection to control the leakage of visible states without relying on any specific nature for  $X$  (see Tbl. I). The key ingredients are: (i) reconstruction of  $e'$  and  $p'$  with good energy and angular resolution; in what follows, we assume unit reconstruction efficiency for  $e'$  and  $p'$  within the  $\eta_{p'}$ ,  $E_{p'}$  and  $Q^2$  kinematic domains; (ii) requiring  $\eta_{X,\text{reco}} < 4$  for the indirectly reconstructed pseudorapidity of the missing final state, for the event to be in the instrumented region; and (iii) a veto on any additional reconstructed activity besides  $e'$  and  $p'$ .

Two distinct selections are summarized in Tbl. I. The *Baseline* choice corresponds to an early EIC running configuration with  $(E_p, E_e) = (100, 10)$  GeV, while the *Optimal* selection uses lower beam energies  $(E_p, E_e) = (41, 5)$  GeV and omits the  $Q^2$  selection, to increase the signal yield and illustrate the maximal possible reach of the EIC, see the SuM. Going forward, the complexity of the MPE search strategy suggests that the selection efficiency could be further optimized using modern machine-learning techniques [65, 66].

**Background suppression.** To quantify the residual background after applying our selections, we generated samples of representative processes with visible final states  $X$  (such as  $\pi^0 \rightarrow \gamma\gamma$ ,  $\rho^0 \rightarrow \pi^+\pi^-$ ,  $\phi \rightarrow K\bar{K}$ , and  $\gamma^* \rightarrow \ell^+\ell^-$ ) and propagated them through a fast simulation of the ePIC detector response using the Baseline energy configuration  $(E_p, E_e) = (100, 10)$  GeV. The fast simulation includes beam energy spread, angular divergence, transport through the beam line, and the currently

understood acceptances and resolutions. It has been benchmarked against full-simulation studies performed for other physics channels [67, 68].

The caveats of the estimate include the absence of a realistic detector threshold and quantifying the acceptance near the edge of the uninstrumented domain  $\eta_X \simeq 4$ . In practice, finite experimental thresholds (e.g., energy threshold in the calorimeters) may reduce the effective veto efficiency, and a quantitative assessment of these effects will require dedicated studies with realistic reconstruction and noise conditions once the detector design and software are finalized. On the other hand, improving the performance of background suppression is clearly possible: tightening the  $\eta_{X,\text{reco}}$  requirement to stay further inside the fully instrumented region, lowering calorimeter thresholds, combining information from multiple subsystems (e.g., trackers and calorimeters), and adding dedicated forward muon and photon detectors in the case of the second EIC detector. These refinements, taken together, would all reduce the leakage probability. Altogether, we regard the background rejection efficiency obtained in this work as conservative.

In the simulation, we classify events according to the *true* pseudorapidity of  $X$ : either  $\eta_X < 4$ , where the detector is fully instrumented, or  $\eta_X > 4$ , where only partial or no coverage is available. For events with  $\eta_X < 4$ , background rejection is limited only by the efficiency of the global veto in the instrumented region. For example, to fully veto all events coming from the dominant  $\pi^0 \rightarrow \gamma\gamma$  background, a veto inefficiency  $\lesssim 10^{-9}$  is required. As a simple and conservative way to achieve such vetoing, it is sufficient that at least one of the photons be absorbed in the electromagnetic calorimetry. An effective depth of order ten radiation lengths in the relevant regions is enough to ensure this, and this requirement is in fact satisfied for the  $\eta_X < 4$  region in ePIC.

Indeed, we find that in simulated events, the decay products rarely escape without causing detectable signals in the tracking and/or calorimeter systems, for both non-muonic and muonic final states, where the latter rely on signals left in the hadronic calorimeters which have  $> 4$  hadronic interaction lengths. Depending on the process, the probability of missing all visible activity in this region is  $10^{-5}$ – $10^{-3}$ , mostly driven by the near-edge events with  $\eta_X \simeq 4$ . Taking into account the caveats in fast simulation discussed above, we render this inefficiency estimate as *conservative*. The corresponding background yield is

$$N_{\text{bg,cons}} \sim 10^5, \quad (2)$$

mainly dominated by the events from  $\rho^0 \rightarrow \pi^+\pi^-$ ,  $\gamma^* \rightarrow \mu^+\mu^-$ , and bremsstrahlung producing a photon. Further details are provided in the SuM.

For events with  $\eta_X > 4$ , contamination of the signal region can only arise if all visible final states escape detection because they traverse uninstrumented or partially instrumented regions *and* if the event is misreconstructed as having  $\eta_{X,\text{reco}} < 4$ . The efficiency of the latter is very high and rapidly increases if tightening it to stay away

$P$	$\text{BR}(P \rightarrow \text{inv})_{\text{current}}$	$\text{BR}(P \rightarrow \text{inv})_{\text{EIC}}$
$\pi^0$	$4.4 \times 10^{-9}$ [43]	$2 \times 10^{-9}$ (Baseline <sub>bg,free</sub> ) $7 \times 10^{-11}$ (Optimal)
$\eta$	$1.1 \times 10^{-4}$ [44]	$2 \times 10^{-6}$ (Baseline <sub>bg,cons</sub> ) $1 \times 10^{-8}$ (Baseline <sub>bg,free</sub> ) $2 \times 10^{-9}$ (Optimal)
$\eta'$	$2.1 \times 10^{-4}$ [44]	$2 \times 10^{-5}$ (Baseline <sub>bg,cons</sub> ) $8 \times 10^{-8}$ (Baseline <sub>bg,free</sub> ) $1 \times 10^{-8}$ (Optimal)

TABLE II. Current experimental bounds on invisible decays of pseudoscalar mesons, obtained by NA64 $_{\pi}$  [44], and the EIC projections. We consider the Baseline and Optimal selection from Tbl. I.

from the boundary of the instrumented region. Additionally, a future improvement could be to achieve a better resolution in the indirect reconstruction of the kinematics of  $X$ . We therefore assume that the only background comes from the  $\eta_X < 4$  domain, with the conservative estimate for the background number given by Eq. (2).

Given the discussion, we present projected sensitivities considering background assumptions: the conservative estimate Eq. (2), and the background-free hypothesis  $N_{\text{bg}} = 0$ . To estimate the reach, we require  $\sum_X N_X \cdot \text{BR}(X \rightarrow \text{inv}) > 2\sqrt{N_{\text{bg}}}$  for the former scenario, and  $\sum_X N_X \cdot \text{BR}(X \rightarrow \text{inv}) > 3$  for the latter, where  $N_X = \mathcal{L} \cdot \sigma_{\text{sel}}$ , with  $\sigma_{\text{sel}}$  being the production cross section of the  $X$  particle after imposing the selection from Tbl. I.

**The pseudoscalar case.** Let us now study the implications of our analysis for the case of invisible decays of pseudoscalar states. These include invisible decays of  $P = \pi^0, \eta, \eta'$ , as well as of hadronically-coupled ALPs  $a$ . We focus on the model of gluonic ALPs:

$$\mathcal{L}_a \supset \frac{\alpha_s}{4\pi} \frac{a}{f_a} G^{\mu\nu} \tilde{G}_{\mu\nu} + ig_{a\chi} a \bar{\chi} \gamma^5 \chi, \quad (3)$$

where  $\tilde{G}_{\mu\nu} \equiv (1/2)\epsilon_{\mu\nu\rho\sigma} G^{\rho\sigma}$ ,  $\chi$  is a dark sector particle, and the ALP mass  $m_a$  is taken to be a free parameter. Motivated by the axion quality problem [69–72], ALPs with masses much larger than the QCD axion  $m_a^2 \gg (m_\pi f_\pi/f_a)^2$ , with  $f_a$  the ALP decay constant, have been considered. Such heavy variants arise in models addressing the strong CP problem [73–90], and have been the focus of extensive theoretical and experimental studies [15, 19, 91–122]. Moreover, we are interested in the regime where  $\text{BR}(a \rightarrow \chi\bar{\chi}) \approx 1$  and the ALP does not decay visibly inside the detector, which is satisfied for most values of  $g_{a\chi}$  due to the relatively small width to visible states  $\Gamma_{a \rightarrow \text{vis.}} \ll m_a \sim \Gamma_{a \rightarrow \chi\bar{\chi}}/g_{a\chi}^2$  [101, 122, 123].

There are two contributions to MPE at the EIC in this model: decays of the on-shell ALP  $X = a \rightarrow \text{inv}$  or of pseudoscalar mesons  $X = P \rightarrow \text{inv}$ , occurring via off-shell ALPs (*i.e.*  $P$ - $a$  mixing), with the main production diagrams of  $X$  particles shown in Fig. 2. Detailed cross-section calculations and kinematics analysis, used in this work, are performed in Ref. [60]. Ear-

lier studies [124–126] computed the cross sections for  $\gamma^{(*)} + p \rightarrow \pi^0 + p$  and calibrated them on pion photoproduction data from DESY, JLAB, and SLAC. Ref. [60] generalizes this framework using the full  $2 \rightarrow 3$  phase-space calculations by including the production of  $\eta^{(*)}$  and ALPs, in a way consistent with the soft-photon theorem [127, 128], which is crucial in the low-momentum-transfer domain  $Q^2 \ll 1 \text{ GeV}^2$  where the cross section saturates. The hadronic couplings of mesons and ALPs are constructed as in Refs. [60, 101, 116, 119, 122, 123].

The signal cross section, namely single pseudoscalar production, can eventually be validated using meson decays into well-measured visible channels, resulting in a smaller theoretical uncertainty on the signal yield. This approach is viable in our case thanks to the reliable reconstruction of the final-state system  $X$  and the good invariant-mass resolution for all visible states. Notably, such a robust data-driven strategy can also facilitate precision measurements of rare Standard Model meson decays.

The EIC reach for invisible decays of  $\pi^0, \eta, \eta'$ , assuming that only a single meson species contributes to the signal yield (which is often true for particular parameters of the model Eq. (3)), is summarized in Tbl. II. For the Baseline selection, we find the improvement for invisible  $\eta^{(*)}$  decays over existing bounds as large as  $\mathcal{O}(10^4)$ . In addition, the EIC sensitivity to  $\pi^0 \rightarrow \text{inv}$  is expected to be  $\sim 2$  times stronger than the current bound. Utilizing the Optimal selection would further improve the sensitivity by a factor of  $\simeq 30$  for  $\pi^0$  and  $\simeq 5 - 8$  for  $\eta^{(*)}$ .

The EIC probes the sum of the on-shell and off-shell ALP contributions in a complementary way, without the ability to disentangle them within a single energy run. The on-shell ALP signal yield scales as  $\text{BR}(a \rightarrow \text{inv})/f_a^2$ , while the off-shell ALP yield scales as  $g_{a\chi}^2/f_a^2$ . Combining this with  $\Gamma_{\text{vis.}} \ll \Gamma_{a \rightarrow \chi\bar{\chi}}/g_{a\chi}^2$ , we find that the on-shell ALP production is the main probe for small values of  $g_{a\chi}$ , while the off-shell ALP dominates for  $g_{a\chi} \sim \mathcal{O}(1)$ . In addition, the ALP mass reach of the two contributions is different as the off-shell production can probe masses above the mother meson at the  $\mathcal{O}(10 \text{ GeV})$  scale, see SuM.

We present the combined sensitivity of the two contributions (on-shell and off-shell) on the  $\{m_a, f_a^{-1}\}$  plane for  $g_{a\chi} = 1(0.01)$ , as well as corresponding bounds, shown in the left (right) panel of Fig. 3, see SuM for details. In particular, the off-shell (on-shell) process dominates the sensitivity for  $g_{a\chi} = 1(10^{-2})$ . Furthermore, we derive the bounds from meson invisible decays resulting from current experimental results on  $K \rightarrow \pi + \text{inv}$  from NA62 [129] and  $\eta^{(*)} \rightarrow \text{inv}$  from NA64h [44] (black region). Additionally, we show the current bounds inferred from the measurements  $K^+ \rightarrow \pi^+ \nu\bar{\nu}$  [131] (brown region) and  $B^+ \rightarrow K^+ \nu\bar{\nu}$  [130, 132–134] (turquoise region).

If a significant excess of MPE events were observed, a more detailed investigation of the signal characteristics (including disentangling multiple contributions) and possible background contributions would be required. Given

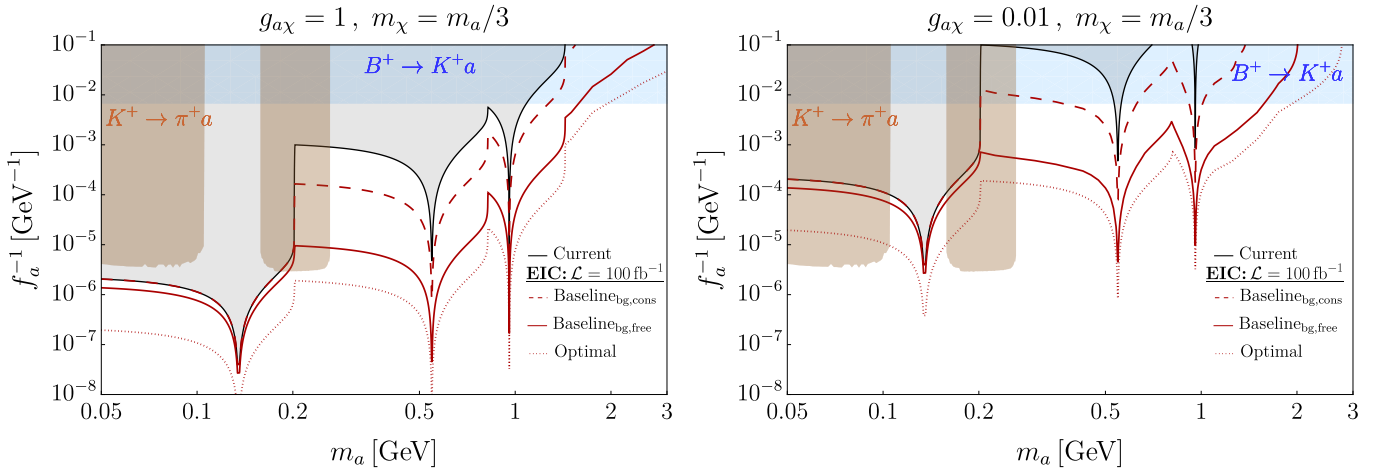


FIG. 3. The EIC projections for invisible ALPs search (see Eq. (3)) in the  $\{m_a, f_a^{-1}\}$  plane, for  $g_{a\chi} = 1$  (0.01) on the left (right) panel. The left (right) panel is dominated by invisible meson (ALP) decay. We use the Baseline selection under conservative (Eq. (2)) and background-free assumptions (dash and solid red), as well as the Optimal selection (red dotted). Current bounds from invisible flavorless meson [43, 44] (black), kaon [129] (brown region) and  $B$ -meson decays [130] (turquoise region) are also presented.

the intrinsic difficulty of reconstructing the missing invariant mass at the EIC, we instead exploit the possibility of varying the incoming beam energies. For example, when considering center-of-mass energies in the range  $\sqrt{s} = 28\text{--}140\text{ GeV}$ , the event rate under the Baseline selection changes in a way that depends on the mass of the missing particle: it is larger by a factor of about 3 for a missing neutral pion than for a missing  $\eta'$ . Moreover, the shapes of the missing energy  $E_X = E_p + E_e - E_{p'} - E_{e'}$  distributions differ significantly for various masses due to different contributions of the intermediate processes in the scattering, as discussed in [60]. We leave the investigation of this question for future work.

**Outlook.** We introduce a new search at the EIC: missing proton energy (MPE), originating from electro-production processes with invisibly decaying final states. In principle, this search may reach the background-free level, while the theoretical uncertainty may be minimized by normalizing the signal yield by the data. We demonstrate its potential by considering the model of axion-like particles coupled to the dark sector, featuring invisibly decaying pseudoscalar mesons,  $\pi^0$  and  $\eta^{(\prime)}$ , with the explored parameter space of axion-like particles well below the current bounds.

Our search strategy can also be utilized for new physics with sizable invisible decay modes, like new spin-1 states, and even for milli-charged particles. Moreover, in case new states have both hadronic and leptonic interactions, e.g., vector particles with anomaly-free couplings, it may be combined with other analyses at the EIC, like the missing-electron-energy search proposed in Ref. [22], to maximize the sensitivity. These possibilities motivate future dedicated studies.

In addition, the MPE motivates a possible detector upgrade at the EIC, including a complementary second

detector [62, 63, 135], to further enhance the sensitivity and disentangle the contributions from the mesons and ALP decays, thereby providing insight into model properties. Taken together, these results show that the EIC can, on the one hand, push the frontiers of precision hadron physics, but also facilitate searches for well-motivated new physics scenarios.

Finally, future lepton-hadron facilities with different energies and/or new beam species – such as the proposed electron-ion collider in China [136], Large Hadron electron Collider [137], Muon (Synchrotron) Ion Collider [120, 138] or  $\mu$ LHC [139] – may also utilize the MPE searches, exploring complementary model parameter regimes and production mechanisms.

## ACKNOWLEDGMENTS

We are grateful to Admir Greljo, Or Hen, Tim Hobbs, Rotem Ovadia, Fernando Romero-López, Miguel Vanvlasselaer, Urs Wiedemann, and Mike Williams for their helpful comments and encouragement. The research of RB is supported in part by the U.S. Department of Energy grant number DE-SC0010107. HL is supported by the U.S. Department of Energy under Grant Contract DE-SC0012704. TC and YS are supported by the ISF (grant No. 597/24) and by BSF (grant No. 2024091). YS thanks CERN-TH for the scientific associateship. ST was supported by the Office of High Energy Physics of the U.S. Department of Energy (DOE) under Grant No. DE-SC0012567, and by the DOE QuantISED program through the theory consortium “Intersections of QIS and Theoretical Particle Physics” at Fermilab (FNAL 20-17). ST is additionally supported

by the Swiss National Science Foundation - project n. PZ00P2.223581, and acknowledges the CERN TH Department for hospitality while this research was being carried out. The work of AJ is supported by the U.S. Department of Energy under Contract DE-SC001270.

This project has also received funding from the European Union's Horizon Europe research and innovation programme under the Marie Skłodowska-Curie Staff Exchange grant agreement No 101086085 - ASYMMETRY.

---

[1] A. Accardi et al., *Electron Ion Collider: The Next QCD Frontier: Understanding the glue that binds us all*, *Eur. Phys. J. A* **52** (2016), no. 9 268, [[arXiv:1212.1701](#)].

[2] R. Abdul Khalek et al., *Science Requirements and Detector Concepts for the Electron-Ion Collider: EIC Yellow Report*, *Nucl. Phys. A* **1026** (2022) 122447, [[arXiv:2103.05419](#)].

[3] M. Gonderinger and M. J. Ramsey-Musolf, *Electron-to-Tau Lepton Flavor Violation at the Electron-Ion Collider*, *JHEP* **11** (2010) 045, [[arXiv:1006.5063](#)]. [Erratum: *JHEP* 05, 047 (2012)].

[4] R. Boughezal, F. Petriello, and D. Wiegand, *Removing flat directions in standard model EFT fits: How polarized electron-ion collider data can complement the LHC*, *Phys. Rev. D* **101** (2020), no. 11 116002, [[arXiv:2004.00748](#)].

[5] Y. Liu and B. Yan, *Searching for the axion-like particle at the EIC\**, *Chin. Phys. C* **47** (2023), no. 4 043113, [[arXiv:2112.02477](#)].

[6] V. Cirigliano, K. Fuyuto, C. Lee, E. Mereghetti, and B. Yan, *Charged Lepton Flavor Violation at the EIC*, *JHEP* **03** (2021) 256, [[arXiv:2102.06176](#)].

[7] H. Davoudiasl, R. Marcarelli, and E. T. Neil, *Lepton-flavor-violating ALPs at the Electron-Ion Collider: a golden opportunity*, *JHEP* **02** (2023) 071, [[arXiv:2112.04513](#)].

[8] B. Yan, Z. Yu, and C. P. Yuan, *The anomalous  $Zbb^-$  couplings at the HERA and EIC*, *Phys. Lett. B* **822** (2021) 136697, [[arXiv:2107.02134](#)].

[9] H. T. Li, B. Yan, and C. P. Yuan, *Jet charge: A new tool to probe the anomalous  $Zbb^-$  couplings at the EIC*, *Phys. Lett. B* **833** (2022) 137300, [[arXiv:2112.07747](#)].

[10] B. Batell, T. Ghosh, T. Han, and K. Xie, *Heavy neutral leptons at the Electron-Ion Collider*, *JHEP* **03** (2023) 020, [[arXiv:2210.09287](#)].

[11] J. L. Zhang et al., *Search for  $e \rightarrow \tau$  charged lepton flavor violation at the EIC with the ECCE detector*, *Nucl. Instrum. Meth. A* **1053** (2023) 168276, [[arXiv:2207.10261](#)].

[12] B. Yan, *Probing the dark photon via polarized DIS scattering at the HERA and EIC*, *Phys. Lett. B* **833** (2022) 137384, [[arXiv:2203.01510](#)].

[13] R. Boughezal, A. Emmert, T. Kutz, S. Mantry, M. Nycz, F. Petriello, K. Simsek, D. Wiegand, and X. Zheng, *Neutral-current electroweak physics and SMEFT studies at the EIC*, *Phys. Rev. D* **106** (2022), no. 1 016006, [[arXiv:2204.07557](#)].

[14] H. Davoudiasl, R. Marcarelli, and E. T. Neil, *Displaced signals of hidden vectors at the Electron-Ion Collider*, *Phys. Rev. D* **108** (2023), no. 7 075017, [[arXiv:2307.00102](#)].

[15] R. Balkin, O. Hen, W. Li, H. Liu, T. Ma, Y. Soreq, and M. Williams, *Probing axion-like particles at the Electron-Ion Collider*, *JHEP* **02** (2024) 123, [[arXiv:2310.08827](#)].

[16] H. Davoudiasl, R. Marcarelli, and E. T. Neil, *Flavor-violating ALPs, electron  $g-2$ , and the Electron-Ion Collider*, *Phys. Rev. D* **109** (2024), no. 11 115013, [[arXiv:2402.17821](#)].

[17] H.-L. Wang, X.-K. Wen, H. Xing, and B. Yan, *Probing the four-fermion operators via the transverse double spin asymmetry at the Electron-Ion Collider*, *Phys. Rev. D* **109** (2024), no. 9 095025, [[arXiv:2401.08419](#)].

[18] X.-K. Wen, B. Yan, Z. Yu, and C. P. Yuan, *Dihadron azimuthal asymmetry and light-quark dipole moments at the Electron-Ion Collider*, [arXiv:2408.07255](#).

[19] Q. Gao, D. Lin, H. Liu, and T. Ma, *Dark photons and axion-like particles at the electron-ion collider in China*, *JHEP* **06** (2025) 070, [[arXiv:2412.06301](#)].

[20] Y. Du, *Parity violation on longitudinal single-spin asymmetries at the EicC*, *Phys. Rev. D* **111** (2025), no. 11 116026, [[arXiv:2412.20469](#)].

[21] Y. Deng, X.-H. Jiang, T. Liu, and B. Yan, *Testing lepton flavor universality at the Electron-Ion Collider*, *JHEP* **06** (2025) 157, [[arXiv:2503.02605](#)].

[22] H. Davoudiasl and H. Liu, *Electron-ion collider as a discovery tool for invisible dark bosons*, *Phys. Rev. D* **112** (2025), no. 7 075001, [[arXiv:2505.08871](#)].

[23] L. Bellafronte, S. Dawson, P. P. Giardino, and H. Liu, *Probing Top Quark - Electron Interactions at Future Colliders*, [arXiv:2507.02039](#).

[24] X.-H. Jiang, Y. Liu, and B. Yan, *Probing top-quark electroweak couplings indirectly at the Electron-Ion Collider*, [arXiv:2507.21477](#).

[25] Y. Huang, X.-B. Tong, and H.-L. Wang, *Nucleon energy correlators as a probe of light-quark dipole operators at the EIC*, [arXiv:2508.08516](#).

[26] A. Jentsch, *Physics Opportunities in the Far-forward Region at the Future Electron-Ion Collider*, *Acta Phys. Pol. B Proc. Suppl.* **16** (2023) 7–A13.

[27] M. Pitt, *Physics Perspectives with the ePIC Far-Forward and Far-Backward detectors*, *PoS DIS2024* (2025) 259, [[arXiv:2409.02811](#)].

[28] D.-N. Gao, *Note on invisible decays of light mesons*, *Phys. Rev. D* **98** (2018), no. 11 113006, [[arXiv:1811.10152](#)].

[29] P. Fayet, *Constraints on Light Dark Matter and  $U$  bosons, from  $\psi$ ,  $\Upsilon$ ,  $K+$ ,  $\pi 0$ ,  $\eta$  and  $\eta'$  decays*, *Phys. Rev. D* **74** (2006) 054034, [[hep-ph/0607318](#)].

[30] J. F. Kamenik and C. Smith, *FCNC portals to the dark sector*, *JHEP* **03** (2012) 090, [[arXiv:1111.6402](#)].

[31] S. N. Gninenco, *Search for invisible decays of  $\pi^0, \eta, \eta', K_S$  and  $K_L$ : A probe of new physics and tests using the Bell-Steinberger relation*, *Phys. Rev. D* **91** (2015), no. 1 015004, [[arXiv:1409.2288](#)].

[32] S. N. Gninenco and N. V. Krasnikov, *Invisible  $K_L$*

decays as a probe of new physics, *Phys. Rev. D* **92** (2015), no. 3 034009, [[arXiv:1503.01595](#)].

[33] S. N. Gninenko and N. V. Krasnikov, *Invisible  $K_L$  decays in the SM extensions*, *Mod. Phys. Lett. A* **31** (2016), no. 25 1650142, [[arXiv:1602.03548](#)].

[34] D. Barducci, M. Fabbrichesi, and E. Gabrielli, *Neutral Hadrons Disappearing into the Darkness*, *Phys. Rev. D* **98** (2018), no. 3 035049, [[arXiv:1806.05678](#)].

[35] M. Hostert, K. Kaneta, and M. Pospelov, *Pair production of dark particles in meson decays*, *Phys. Rev. D* **102** (2020), no. 5 055016, [[arXiv:2005.07102](#)].

[36] REDTOP Collaboration, J. Elam et al., *The REDTOP experiment: Rare  $\eta/\eta'$  Decays To Probe New Physics*, [arXiv:2203.07651](#).

[37] T. Li, X.-D. Ma, and M. A. Schmidt, *General neutrino interactions with sterile neutrinos in light of coherent neutrino-nucleus scattering and meson invisible decays*, *JHEP* **07** (2020) 152, [[arXiv:2005.01543](#)].

[38] B. McElrath, *Invisible quarkonium decays as a sensitive probe of dark matter*, *Phys. Rev. D* **72** (2005) 103508, [[hep-ph/0506151](#)].

[39] B. Batell, P. deNiverville, D. McKeen, M. Pospelov, and A. Ritz, *Leptophobic Dark Matter at Neutrino Factories*, *Phys. Rev. D* **90** (2014), no. 11 115014, [[arXiv:1405.7049](#)].

[40] B. Batell, A. Freitas, A. Ismail, and D. McKeen, *Probing Light Dark Matter with a Hadrophilic Scalar Mediator*, *Phys. Rev. D* **100** (2019), no. 9 095020, [[arXiv:1812.05103](#)].

[41] L. Darmé, S. A. R. Ellis, and T. You, *Light Dark Sectors through the Fermion Portal*, *JHEP* **07** (2020) 053, [[arXiv:2001.01490](#)].

[42] Y. Ema, F. Sala, and R. Sato, *Neutrino experiments probe hadrophilic light dark matter*, *SciPost Phys.* **10** (2021), no. 3 072, [[arXiv:2011.01939](#)].

[43] NA62 Collaboration, E. Cortina Gil et al., *Search for  $\pi^0$  decays to invisible particles*, *JHEP* **02** (2021) 201, [[arXiv:2010.07644](#)].

[44] NA64 Collaboration, Y. M. Andreev et al., *Dark-Sector Search via Pion-Produced  $\eta$  and  $\eta'$  Mesons Decaying Invisibly in the NA64h Detector*, *Phys. Rev. Lett.* **133** (2024), no. 12 121803, [[arXiv:2406.01990](#)].

[45] R. D. Peccei and H. R. Quinn, *CP Conservation in the Presence of Instantons*, *Phys. Rev. Lett.* **38** (1977) 1440–1443.

[46] R. D. Peccei and H. R. Quinn, *Constraints Imposed by CP Conservation in the Presence of Instantons*, *Phys. Rev. D* **16** (1977) 1791–1797.

[47] S. Weinberg, *A New Light Boson?*, *Phys. Rev. Lett.* **40** (1978) 223–226.

[48] F. Wilczek, *Problem of Strong  $P$  and  $T$  Invariance in the Presence of Instantons*, *Phys. Rev. Lett.* **40** (1978) 279–282.

[49] L. F. Abbott and P. Sikivie, *A Cosmological Bound on the Invisible Axion*, *Phys. Lett. B* **120** (1983) 133–136.

[50] M. Dine and W. Fischler, *The Not So Harmless Axion*, *Phys. Lett. B* **120** (1983) 137–141.

[51] J. Preskill, M. B. Wise, and F. Wilczek, *Cosmology of the Invisible Axion*, *Phys. Lett. B* **120** (1983) 127–132.

[52] D. J. E. Marsh, *Axion Cosmology*, *Phys. Rept.* **643** (2016) 1–79, [[arXiv:1510.07633](#)].

[53] C. B. Adams et al., *Axion Dark Matter*, in *Snowmass 2021*, 3, 2022. [arXiv:2203.14923](#).

[54] Y. Nomura and J. Thaler, *Dark Matter through the Axion Portal*, *Phys. Rev. D* **79** (2009) 075008, [[arXiv:0810.5397](#)].

[55] M. Freytsis and Z. Ligeti, *On dark matter models with uniquely spin-dependent detection possibilities*, *Phys. Rev. D* **83** (2011) 115009, [[arXiv:1012.5317](#)].

[56] M. J. Dolan, F. Kahlhoefer, C. McCabe, and K. Schmidt-Hoberg, *A taste of dark matter: Flavour constraints on pseudoscalar mediators*, *JHEP* **03** (2015) 171, [[arXiv:1412.5174](#)]. [Erratum: *JHEP* 07, 103 (2015)].

[57] Y. Hochberg, E. Kuflik, R. McGehee, H. Murayama, and K. Schutz, *Strongly interacting massive particles through the axion portal*, *Phys. Rev. D* **98** (2018), no. 11 115031, [[arXiv:1806.10139](#)].

[58] P. J. Fitzpatrick, Y. Hochberg, E. Kuflik, R. Ovadia, and Y. Soreq, *Dark matter through the axion-gluon portal*, *Phys. Rev. D* **108** (2023), no. 7 075003, [[arXiv:2306.03128](#)].

[59] Z. S. Wang, Y. Zhang, and W. Liu, *Searching for heavy neutral leptons coupled to axion-like particles at the LHC far detectors and SHiP*, *JHEP* **01** (2025) 070, [[arXiv:2409.18424](#)].

[60] R. Balkin, T. Coren, A. Jentsch, H. Liu, M. Ovchynnikov, Y. Soreq, and S. Trifinopoulos, *In Preparation*.

[61] ePIC Collaboration, “The epic detector and collaboration.” <https://www.bnl.gov/eic/epic.php>, 2025.

[62] V. Burkert et al., *Precision studies of qcd in the low energy domain of the eic*, *Progress in Particle and Nuclear Physics* **131** (2023) 104032.

[63] P. Nadel-Turonski, *A Second Detector for the Electron-Ion Collider*, *PoS DIS2024* (2024) 283.

[64] E. C. Aschenauer, A. Bazilevsky, A. Jentsch, J. Kim, A. Kiselev, B. S. Page, Z. Tu, T. Ullrich, and C. P. Wong, *Tagging efficiency study of incoherent diffractive vector meson production at the second interaction region at the electron-ion collider*, *Phys. Rev. D* **111** (Apr, 2025) 072013.

[65] C. Allaire et al., *Artificial Intelligence for the Electron Ion Collider (AI4EIC)*, *Comput. Softw. Big Sci.* **8** (2024) 5, [[arXiv:2307.08593](#)].

[66] J. Y. Araz, V. Mikuni, F. Ringer, N. Sato, F. T. Acosta, and R. Whitehill, *Point cloud-based diffusion models for the Electron-Ion Collider*, *Phys. Lett. B* **868** (2025) 139694, [[arXiv:2410.22421](#)].

[67] A. Jentsch, Z. Tu, and C. Weiss, *Deep-inelastic electron-deuteron scattering with spectator nucleon tagging at the future electron ion collider: Extracting free nucleon structure*, *Phys. Rev. C* **104** (Dec, 2021) 065205.

[68] E. C. Aschenauer, V. Batozskaya, S. Fazio, A. Jentsch, J. Kim, K. Kumerički, H. Moutarde, K. Passek-K., D. Sokhan, H. Spiesberger, P. Sznajder, and K. Tezgin, *Study of deeply virtual compton scattering at the future electron-ion collider*, *Phys. Rev. D* **112** (Aug, 2025) 036010.

[69] M. Kamionkowski and J. March-Russell, *Planck scale physics and the Peccei-Quinn mechanism*, *Phys. Lett. B* **282** (1992) 137–141, [[hep-th/9202003](#)].

[70] R. Holman, S. D. H. Hsu, T. W. Kephart, E. W. Kolb, R. Watkins, and L. M. Widrow, *Solutions to the strong CP problem in a world with gravity*, *Phys. Lett. B* **282** (1992) 132–136, [[hep-ph/9203206](#)].

[71] S. M. Barr and D. Seckel, *Planck scale corrections to axion models*, *Phys. Rev. D* **46** (1992) 539–549.

[72] S. Ghigna, M. Lusignoli, and M. Roncadelli, *Instability of the invisible axion*, *Phys. Lett. B* **283** (1992) 278–281.

[73] S. Dimopoulos, *A Solution of the Strong CP Problem in Models With Scalars*, *Phys. Lett. B* **84** (1979) 435–439.

[74] B. Holdom and M. E. Peskin, *Raising the Axion Mass*, *Nucl. Phys. B* **208** (1982) 397–412.

[75] J. M. Flynn and L. Randall, *A Computation of the Small Instanton Contribution to the Axion Potential*, *Nucl. Phys. B* **293** (1987) 731–739.

[76] V. A. Rubakov, *Grand unification and heavy axion*, *JETP Lett.* **65** (1997) 621–624, [[hep-ph/9703409](#)].

[77] Z. Berezhiani, L. Gianfagna, and M. Giannotti, *Strong CP problem and mirror world: The Weinberg-Wilczek axion revisited*, *Phys. Lett. B* **500** (2001) 286–296, [[hep-ph/0009290](#)].

[78] H. Fukuda, K. Harigaya, M. Ibe, and T. T. Yanagida, *Model of visible QCD axion*, *Phys. Rev. D* **92** (2015), no. 1 015021, [[arXiv:1504.06084](#)].

[79] T. Gherghetta, N. Nagata, and M. Shifman, *A Visible QCD Axion from an Enlarged Color Group*, *Phys. Rev. D* **93** (2016), no. 11 115010, [[arXiv:1604.01127](#)].

[80] S. Dimopoulos, A. Hook, J. Huang, and G. Marques-Tavares, *A collider observable QCD axion*, *JHEP* **11** (2016) 052, [[arXiv:1606.03097](#)].

[81] H. Fukuda, M. Ibe, and T. T. Yanagida, *Dark Matter Candidates in a Visible Heavy QCD Axion Model*, *Phys. Rev. D* **95** (2017), no. 9 095017, [[arXiv:1702.00227](#)].

[82] P. Agrawal and K. Howe, *Factoring the Strong CP Problem*, *JHEP* **12** (2018) 029, [[arXiv:1710.04213](#)].

[83] M. K. Gaillard, M. B. Gavela, R. Houtz, P. Quilez, and R. Del Rey, *Color unified dynamical axion*, *Eur. Phys. J. C* **78** (2018), no. 11 972, [[arXiv:1805.06465](#)].

[84] B. Lillard and T. M. P. Tait, *A High Quality Composite Axion*, *JHEP* **11** (2018) 199, [[arXiv:1811.03089](#)].

[85] A. Hook, S. Kumar, Z. Liu, and R. Sundrum, *High Quality QCD Axion and the LHC*, *Phys. Rev. Lett.* **124** (2020), no. 22 221801, [[arXiv:1911.12364](#)].

[86] C. Csáki, M. Ruhdorfer, and Y. Shirman, *UV Sensitivity of the Axion Mass from Instantons in Partially Broken Gauge Groups*, *JHEP* **04** (2020) 031, [[arXiv:1912.02197](#)].

[87] T. Gherghetta, V. V. Khoze, A. Pomarol, and Y. Shirman, *The Axion Mass from 5D Small Instantons*, *JHEP* **03** (2020) 063, [[arXiv:2001.05610](#)].

[88] A. Valenti, L. Vecchi, and L.-X. Xu, *Grand Color axion*, *JHEP* **10** (2022) 025, [[arXiv:2206.04077](#)].

[89] A. Kivel, J. Laux, and F. Yu, *Supersizing axions with small size instantons*, *JHEP* **11** (2022) 088, [[arXiv:2207.08740](#)].

[90] D. I. Dunsky, L. J. Hall, and K. Harigaya, *A heavy QCD axion and the mirror world*, *JHEP* **02** (2024) 212, [[arXiv:2302.04274](#)].

[91] M. J. Dolan, T. Ferber, C. Hearty, F. Kahlhoefer, and K. Schmidt-Hoberg, *Revised constraints and Belle II sensitivity for visible and invisible axion-like particles*, *JHEP* **12** (2017) 094, [[arXiv:1709.00009](#)]. [Erratum: *JHEP* 03, 190 (2021)].

[92] D. S. M. Alves and N. Weiner, *A viable QCD axion in the MeV mass range*, *JHEP* **07** (2018) 092, [[arXiv:1710.03764](#)].

[93] W. J. Marciano, A. Masiero, P. Paradisi, and M. Passera, *Contributions of axionlike particles to lepton dipole moments*, *Phys. Rev. D* **94** (2016), no. 11 115033, [[arXiv:1607.01022](#)].

[94] J. Jaeckel and M. Spannowsky, *Probing MeV to 90 GeV axion-like particles with LEP and LHC*, *Phys. Lett. B* **753** (2016) 482–487, [[arXiv:1509.00476](#)].

[95] B. Döbrich, J. Jaeckel, F. Kahlhoefer, A. Ringwald, and K. Schmidt-Hoberg, *ALPtraum: ALP production in proton beam dump experiments*, *JHEP* **02** (2016) 018, [[arXiv:1512.03069](#)].

[96] E. Izaguirre, T. Lin, and B. Shuve, *Searching for Axionlike Particles in Flavor-Changing Neutral Current Processes*, *Phys. Rev. Lett.* **118** (2017), no. 11 111802, [[arXiv:1611.09355](#)].

[97] S. Knapen, T. Lin, H. K. Lou, and T. Melia, *Searching for Axionlike Particles with Ultraperipheral Heavy-Ion Collisions*, *Phys. Rev. Lett.* **118** (2017), no. 17 171801, [[arXiv:1607.06083](#)].

[98] M. Bauer, M. Heiles, M. Neubert, and A. Thamm, *Axion-Like Particles at Future Colliders*, *Eur. Phys. J. C* **79** (2019), no. 1 74, [[arXiv:1808.10323](#)].

[99] A. Mariotti, D. Redigolo, F. Sala, and K. Tobioka, *New LHC bound on low-mass diphoton resonances*, *Phys. Lett. B* **783** (2018) 13–18, [[arXiv:1710.01743](#)].

[100] X. Cid Vidal, A. Mariotti, D. Redigolo, F. Sala, and K. Tobioka, *New Axion Searches at Flavor Factories*, *JHEP* **01** (2019) 113, [[arXiv:1810.09452](#)]. [Erratum: *JHEP* 06, 141 (2020)].

[101] D. Aloni, Y. Soreq, and M. Williams, *Coupling QCD-Scale Axionlike Particles to Gluons*, *Phys. Rev. Lett.* **123** (2019), no. 3 031803, [[arXiv:1811.03474](#)].

[102] D. Aloni, C. Fanelli, Y. Soreq, and M. Williams, *Photoproduction of Axionlike Particles*, *Phys. Rev. Lett.* **123** (2019), no. 7 071801, [[arXiv:1903.03586](#)].

[103] M. Bauer, M. Neubert, S. Renner, M. Schnubel, and A. Thamm, *The Low-Energy Effective Theory of Axions and ALPs*, *JHEP* **04** (2021) 063, [[arXiv:2012.12272](#)].

[104] M. Bauer, M. Neubert, S. Renner, M. Schnubel, and A. Thamm, *Consistent Treatment of Axions in the Weak Chiral Lagrangian*, *Phys. Rev. Lett.* **127** (2021), no. 8 081803, [[arXiv:2102.13112](#)].

[105] Y. Sakaki and D. Ueda, *Searching for new light particles at the international linear collider main beam dump*, *Phys. Rev. D* **103** (2021), no. 3 035024, [[arXiv:2009.13790](#)].

[106] A. Flórez, A. Gurrola, W. Johns, P. Sheldon, E. Sheridan, K. Sinha, and B. Soubasis, *Probing axionlike particles with  $\gamma\gamma$  final states from vector boson fusion processes at the LHC*, *Phys. Rev. D* **103** (2021), no. 9 095001, [[arXiv:2101.11119](#)].

[107] V. Brdar, B. Dutta, W. Jang, D. Kim, I. M. Shoemaker, Z. Tabrizi, A. Thompson, and J. Yu, *Axionlike Particles at Future Neutrino Experiments: Closing the Cosmological Triangle*, *Phys. Rev. Lett.* **126** (2021), no. 20 201801, [[arXiv:2011.07054](#)].

[108] E. Bertholet, S. Chakraborty, V. Loladze, T. Okui, A. Soffer, and K. Tobioka, *Heavy QCD axion at Belle II: Displaced and prompt signals*, *Phys. Rev. D* **105** (2022), no. 7 L071701, [[arXiv:2108.10331](#)].

[109] R. T. Co, S. Kumar, and Z. Liu, *Searches for heavy*

*QCD axions via dimuon final states, JHEP* **02** (2023) 111, [[arXiv:2210.02462](#)].

[110] S. Trifinopoulos and M. Vanvlasselaer, *Attracting the electroweak scale to a tachyonic trap, Phys. Rev. D* **107** (2023), no. 7 L071701, [[arXiv:2210.13484](#)].

[111] F. A. Ghebretinsaee, Z. S. Wang, and K. Wang, *Probing axion-like particles coupling to gluons at the LHC, JHEP* **07** (2022) 070, [[arXiv:2203.01734](#)].

[112] G. Dalla Valle Garcia, F. Kahlhoefer, M. Ovchynnikov, and A. Zaporozhchenko, *Phenomenology of axionlike particles with universal fermion couplings revisited, Phys. Rev. D* **109** (2024), no. 5 055042, [[arXiv:2310.03524](#)].

[113] Y. Kyselov, S. Mrenna, and M. Ovchynnikov, *New physics particles mixing with mesons: Production in the fragmentation chain, Phys. Rev. D* **112** (2025), no. 5 055033, [[arXiv:2504.06828](#)].

[114] Y. Afik, B. Döbrich, J. Jerhot, Y. Soreq, and K. Tobioka, *Probing long-lived axions at the KOTO experiment, Phys. Rev. D* **108** (2023), no. 5 055007, [[arXiv:2303.01521](#)].

[115] R. Balkin, M. W. Krasny, T. Ma, B. R. Safdi, and Y. Soreq, *Probing Axion-Like-Particles at the CERN Gamma Factory, Annalen Phys.* **534** (2022), no. 3 2100222, [[arXiv:2105.15072](#)].

[116] N. Blinov, E. Kowalczyk, and M. Wynne, *Axion-like particle searches at DarkQuest, JHEP* **02** (2022) 036, [[arXiv:2112.09814](#)].

[117] Z. Bai et al., *New physics searches with an optical dump at LUXE, Phys. Rev. D* **106** (2022), no. 11 115034, [[arXiv:2107.13554](#)].

[118] J. R. Pybus et al., *Search for axion-like particles through nuclear Primakoff production using the GlueX detector, Phys. Lett. B* **855** (2024) 138790, [[arXiv:2308.06339](#)].

[119] Y. Bai, T.-K. Chen, J. Liu, and X. Ma, *Wess-Zumino-Witten Interactions of Axions, Phys. Rev. Lett.* **134** (2025), no. 8 081803, [[arXiv:2406.11948](#)].

[120] H. Davoudiasl, H. Liu, R. Marcarelli, Y. Soreq, and S. Trifinopoulos, *New physics at the Muon (Synchrotron) Ion Collider: MuSIC for several scales, JHEP* **03** (2025) 046, [[arXiv:2412.13289](#)].

[121] C. Baruch, P. J. Fitzpatrick, T. Menzo, Y. Soreq, S. Trifinopoulos, and J. Zupan, *Searching for exotic scalars at fusion reactors, JHEP* **10** (2025) 215, [[arXiv:2502.12314](#)].

[122] M. Ovchynnikov and A. Zaporozhchenko, *Advancing the phenomenology of GeV-scale axionlike particles, Phys. Rev. D* **112** (2025), no. 1 015001, [[arXiv:2501.04525](#)].

[123] R. Balkin, T. Coren, Y. Soreq, and M. Williams, *A covariant description of the interactions of axion-like particles and hadrons, arXiv:2506.15637*.

[124] R. M. Davidson and R. Workman, *Form-factors and photoproduction amplitudes, Phys. Rev. C* **63** (2001) 025210, [[nucl-th/0101066](#)].

[125] M. M. Kaskulov and U. Mosel, *Deep exclusive charged  $\pi$  electroproduction above the resonance region, Phys. Rev. C* **81** (2010) 045202, [[arXiv:1001.1952](#)].

[126] M. M. Kaskulov, *Neutral pion electroproduction in  $p(e, e'\pi^0)p$  above  $\sqrt{s} > 2$  GeV, arXiv:1105.1993*.

[127] F. E. Low, *Bremsstrahlung of very low-energy quanta in elementary particle collisions, Phys. Rev.* **110** (1958) 974–977.

[128] T. H. Burnett and N. M. Kroll, *Extension of the low soft photon theorem, Phys. Rev. Lett.* **20** (1968) 86.

[129] **NA62** Collaboration, E. Cortina Gil et al., *Searches for hidden sectors using  $K^+ \rightarrow \pi^+ X$  decays, JHEP* **11** (2025) 143, [[arXiv:2507.17286](#)].

[130] **Belle-II** Collaboration, I. Adachi et al., *Evidence for  $B \rightarrow K + \nu \bar{\nu}$  decays, Phys. Rev. D* **109** (2024), no. 11 112006, [[arXiv:2311.14647](#)].

[131] **NA62** Collaboration, E. Cortina Gil et al., *Measurement of the very rare  $K^+ \rightarrow \pi^+ \nu \bar{\nu}$  decay, JHEP* **06** (2021) 093, [[arXiv:2103.15389](#)].

[132] S. Chakraborty, M. Kraus, V. Loladze, T. Okui, and K. Tobioka, *Heavy QCD axion in  $b \rightarrow s$  transition: Enhanced limits and projections, Phys. Rev. D* **104** (2021), no. 5 055036, [[arXiv:2102.04474](#)]. [Erratum: Phys. Rev. D 108, 039903 (2023)].

[133] W. Altmannshofer, A. Crivellin, H. Haigh, G. Inguglia, and J. Martin Camalich, *Light new physics in  $B \rightarrow K^*(\nu \bar{\nu})$ ?, Phys. Rev. D* **109** (2024), no. 7 075008, [[arXiv:2311.14629](#)].

[134] M. Abumusabih, G. Dujany, D. Guadagnoli, A. Iohner, and C. Toni, *The  $B^+ \rightarrow K^+ \nu \bar{\nu}$  decay as a search for the QCD axion, arXiv:2510.18953*.

[135] W. Chang, E.-C. Aschenauer, A. Jentsch, A. Kumar, Z. Tu, and Z. Yin, *Opportunities for Imaging Light Nuclei with a Second Interaction Region at the Electron-Ion Collider, arXiv:2511.05638*.

[136] D. P. Anderle et al., *Electron-ion collider in China, Front. Phys. (Beijing)* **16** (2021), no. 6 64701, [[arXiv:2102.09222](#)].

[137] **LHeC, FCC-he Study Group** Collaboration, P. Agostini et al., *The Large Hadron-Electron Collider at the HL-LHC, J. Phys. G* **48** (2021), no. 11 110501, [[arXiv:2007.14491](#)].

[138] D. Acosta, E. Barberis, N. Hurley, W. Li, O. Miguel Colin, Y. Wang, D. Wood, and X. Zuo, *The potential of a TeV-scale muon-ion collider, JINST* **18** (2023), no. 09 P09025, [[arXiv:2203.06258](#)].

[139] D. Akturk et al.,  *$\mu$ LHC: Antimuon Ring and HL-LHC based  $\mu^+ p$  Collider, arXiv:2506.15445*.

[140] J. Alwall, R. Frederix, S. Frixione, V. Hirschi, F. Maltoni, O. Mattelaer, H. S. Shao, T. Stelzer, P. Torrielli, and M. Zaro, *The automated computation of tree-level and next-to-leading order differential cross sections, and their matching to parton shower simulations, JHEP* **07** (2014) 079, [[arXiv:1405.0301](#)].

[141] A. Alloul, N. D. Christensen, C. Degrande, C. Duhr, and B. Fuks, *FeynRules 2.0 - A complete toolbox for tree-level phenomenology, Comput. Phys. Commun.* **185** (2014) 2250–2300, [[arXiv:1310.1921](#)].

[142] N. D. Christensen and C. Duhr, *FeynRules - Feynman rules made easy, Comput. Phys. Commun.* **180** (2009) 1614–1641, [[arXiv:0806.4194](#)].

[143] ePIC Collaboration, “Simulation framework for the epic collaboration.” <https://github.com/eic/epic>, 2020.

[144] S. N. Gninenco, D. V. Kirpichnikov, S. Kuleshov, V. E. Lyubovitskij, and A. S. Zhevlakov, *Test of the vector portal with dark fermions in the charge-exchange reactions in the NA64 experiment at CERN SPS, Phys. Rev. D* **109** (2024), no. 7 075021, [[arXiv:2312.01703](#)].

## SUPPLEMENTAL MATERIAL

In this Supplemental Material, we provide technical details on the calculations of event rates and sensitivity of the EIC. Sec. A is devoted to discussing the Standard Model (SM) backgrounds for the missing-proton-energy (MPE) search at the Electron-Ion Collider (EIC). In Sec. B, we discuss the impact of the Baseline selection (Tbl. I of the main text) on the event yield, highlighting in particular the effect of the  $Q^2$  cut and the role of the beam energies in maximizing the signal-to-background ratio. Sec. C discusses details about the two contributions to the MPE signature at the EIC for the ALP model (ALP decays and pseudoscalar meson decays via off-shell ALPs). In particular, it presents the expression for the branching of invisible decays of pseudoscalar mesons via the ALPs with an arbitrary coupling pattern, and discusses the complementarity between the ALP and meson decays. Finally, in Sec. D, we estimate the bounds on the ALP model from ALP-on-shell and ALP-off-shell decays from NA62 and NA64.

### Appendix A: Further details on backgrounds

In this section, we discuss various background sources for the MPE searches, including irreducible backgrounds, events from physical processes that may mimic the missing decays, and possible instrumental sources. The main purpose of the discussion is to demonstrate that the background can be well-controlled with the currently planned setup of the EIC detector. We also discuss ways in which it can be improved, either via selection criteria or different experimental considerations. Throughout this section, we consider the Baseline selection from Tbl. I, corresponding to the energy configuration with  $E_p = 100 \text{ GeV}$  and  $E_e = 10 \text{ GeV}$ .

#### 1. Irreducible backgrounds

An *irreducible* background comes from the events of the type

$$ep \rightarrow ep + \nu\bar{\nu}/2(\nu\bar{\nu}). \quad (\text{A1})$$

Such events may be either direct (with the off-shell  $Z$  boson), or involve an intermediate on-shell resonance  $X = \{\pi^0, \eta^{(\prime)}, \rho^0, \dots\}$ , which then decays to neutrinos via its mixing with the  $Z$  boson. Using naive dimensional analysis, we estimate  $\sigma \sim G_F^2 s_{\nu\nu} \alpha_{\text{EM}}^2 / [24 \cdot (4\pi)^3]$ , with  $s_{\nu\nu} < s_{ep}$  being the invariant mass of the collision. It gives us  $< 1$  event for  $\mathcal{L}_{\text{int}} = 100 \text{ fb}^{-1}$ . We confirm this by simulating the corresponding inelastic scattering process in MadGraph5\_aMC@NLO [140], and obtaining the total cross section  $\sigma(ep \rightarrow ep\nu\bar{\nu}) \sim 3 \times 10^{-4} \text{ fb}$ . As for the decays via intermediate particles (e.g.,  $\rho^0 \rightarrow \nu\bar{\nu}$ ), the invisible branching ratios of various mesons are at

the level of  $10^{-11}$  or smaller [28], which also implies  $< 1$  events per full EIC running time. Therefore, we conclude that the irreducible background is negligible.

#### 2. Particle leakage

**Leakage sources and partial instrumentation.** Another class of background events consists of low- $Q^2$  processes with emission of the visible states that escape detection. It can be a result of an uninstrumented domain of the detector or of imperfections in the detection of activity in the instrumented region.

Let us first describe the instrumentation. Besides the proton, charged-particle reconstruction may be reliable up to pseudorapidities  $\eta \approx 6$ . However, in the domain  $4.5 \lesssim \eta \lesssim 6$ , the FFD provides only partial azimuthal coverage  $|\Delta\phi_{\text{FFD}}|/2\pi \sim 0.5$ . The higher- $\eta$  region is generally off-limits for other charged particles because they must pass through the hadron beam line to reach the FFDs. In practice, charged particles with mass different than the proton mass and/or with momentum less than about 40% of the primary beam momentum are generally not seen in the FFDs, due to their different magnetic rigidity as they traverse the beam-line magnets.

Neutral-particle detection in the forward hemisphere is nearly hermetic thanks to the FFD calorimeters. In particular, forward photons achieve near-optimal efficiency for  $\eta \gtrsim 6$ . In the domain  $4.5 \lesssim \eta \lesssim 6$ , the same partial azimuthal coverage noted for charged particles applies, and in the window  $4 < \eta < 4.5$  the coverage vanishes completely. At  $|\eta| < 4$ , particles may instead be reconstructed by the mid- $\eta$  detectors.

As discussed in the main text, such a background is reduced by the selection from Tbl. I of the main text. The selection suppresses particle leakage through uninstrumented regions, while the events in the instrumented regions may be vetoed if requiring zero activity behind the outgoing electron and proton, including displaced deposits from decays of long-lived strange states.

As discussed in the main text,  $\eta_X$  can be reliably reconstructed in ePIC via the kinematics of  $e', p'$  with a resolution of  $\sim 5\%$ , which allows for eliminating the backgrounds from the uninstrumented region  $\eta_X > 4$ , where visible  $X$  may escape detection. Finite resolution effects can easily be mitigated by taking a slightly tighter cut on  $\eta_X$ , which only has a small effect on the signal efficiency. Once left with events that truly lie within the instrumented region, the only remaining source of leakage (*i.e.* vetoing inefficiency) is due to the particle detection efficiencies of the detector system, to be discussed below.

**Contributing processes and the vetoing inefficiency in  $\eta < 4$  region.** Given the range of detectable  $Q^2$  we consider, and also the fact that the probability of having such fake-invisible events decreases with the final state multiplicity, the processes causing backgrounds are

Final state $X$	$\sigma_{\text{sel}}$ [fb]	$\sigma_{\text{sel+ineff}}$ [fb]
$\gamma$	$2 \times 10^5$	$4 \times 10^2$
$\gamma^* \rightarrow e^+ e^-$	$\sim 10^4$	$\sim 5 \times 10^{-2}$
$\gamma^* \rightarrow \mu^+ \mu^-$	$4 \times 10^4$	$1 \times 10^2$
$\pi^0 \rightarrow \gamma \gamma$	$2 \times 10^7$	80
$\pi^0 \rightarrow e^+ e^-$	1	$4 \times 10^{-6}$
$\eta \rightarrow \mu^+ \mu^-$	10	$3 \times 10^{-2}$
$\rho^0 \rightarrow \pi^+ \pi^-$	$2 \times 10^7$	$5 \times 10^2$
$\phi \rightarrow KK$	$7 \times 10^5$	10

TABLE S1. Cross sections for various quasi-elastic processes after imposing the Baseline selection from Tbl. I (second column) and if additionally multiplying by the vetoing inefficiency  $\epsilon_{\text{ineff}}$ , see text for details. The number of events per full EIC run may be obtained by multiplying the cross sections by the total luminosity  $\mathcal{L} = 100 \text{ fb}^{-1}$ .

coherent exclusive photoproduction. They include

$$e + p \rightarrow e + p + M, \quad M \rightarrow \text{vis.}, \quad (\text{A2})$$

$$e + p \rightarrow e + p + \gamma, \quad (\text{A3})$$

$$e + p \rightarrow e + p + \gamma^* \rightarrow e + p + \ell^+ + \ell^-, \quad (\text{A4})$$

$$e + p \rightarrow e + p + N + \bar{N}, \quad (\text{A5})$$

where  $M$  is a meson decaying into any visible final state (e.g.,  $\pi^0 \rightarrow \gamma \gamma$ ,  $\eta \rightarrow \mu^+ \mu^-$ ,  $\rho^0 \rightarrow \pi^+ \pi^-$ ,  $\phi \rightarrow KK$ , etc.) and  $N$  is a nucleon. Qualitatively, these processes may be classified into those with neutral non-hadronic states, electron-positron and muon-antimuon pairs, charged light hadronic particles, states with strange mesons, and heavy hadronic states.

To test the efficiency of the Baseline selection in the  $\eta_X < 4$  domain, we proceed as follows. First, we compute the rates of the processes Eqs. (A3)–(A4) by calculating their total cross sections and the fraction of events that survive the selection.

The cross sections for the meson-production processes Eq. (A2) are obtained using the methodology of Ref. [60]. We consider  $\pi^0 \rightarrow \gamma \gamma/e^+ e^-$ ,  $\eta \rightarrow \mu^+ \mu^-$ , as well as  $\rho^0 \rightarrow \pi^+ \pi^-$  and  $\phi \rightarrow K^+ K^- / K_L K_S$ . As for pair production via  $\gamma^*$  and bremsstrahlung producing  $\gamma$ , Eqs. (A3), (A4), we generate the kinematics of the corresponding processes using `MADGRAPH5_AMC@NLO` [140] with a `FEYNRULES` implementation [141, 142], treating the proton as a point-like particle; this approximation is adequate in the relevant  $Q^2$  range. Most of the total cross section of these processes (before imposing any cuts) is dominated by the very soft final state particles  $\gamma, \ell^+ \ell^-$ , and the energy-based selection reduces it by a few orders of magnitude.

Finally, processes of the type (A5) require a large invariant-mass transfer and are expected to be subdominant compared to the other channels; we therefore do not consider them in detail and list them only for completeness.

The resulting yields, reported in the second column of Tbl. S1, correspond to the number of events after the Baseline selection *before any detector-activity veto*. Per

full EIC run,  $\mathcal{L} = 100 \text{ fb}^{-1}$ , they are at the level of:  $\simeq 10^9$  events for the neutral final states (set by the  $\pi^0 \rightarrow \gamma \gamma$  process),  $\simeq 10^9$  events for the charged non-muonic final states (set by  $\rho^0 \rightarrow \pi^+ \pi^-$ ), and  $\simeq 10^6$  for the muonic final states (set by the  $\gamma^* \rightarrow \mu^+ \mu^-$  process).

Next, to evaluate the efficiency of vetoing these remaining events in the planned ePIC setup, we generate event samples for several processes with  $\eta_X < 4$  belonging to the instrumented regions, to process them with a parametrized fast simulation of ePIC, validated using the ePIC software framework [143], similar to Ref. [68]. The processing mimics detector-level and event reconstruction effects: it adds beam-related effects such as energy spread and angular divergence, particle transport, and finite reconstruction efficiencies. It should be noted that it is likely that a full simulation of the ePIC detector will *improve* the resulting vetoing efficiency due to handling of hits in multiple subsystems, rather than efficiencies based on basic knowledge of fiducial acceptance and calorimeter depths.

For each process, we generate  $N_{\text{sample}} = 10^6$  events using `MADGRAPH` and estimate the effect of the kinematic cuts by imposing all relevant pre-selections on lab-frame quantities (e.g. energies). We can then use the resulting distributions to estimate channel-specific particle detection efficiencies as discussed above. However, in practice, we use only the sample from the decaying-meson channel (A2) which contains a sufficient number of events. Due to the limitations of `MADGRAPH`, generating a comparable sample size for (A3) and (A4) would be computationally very expensive. Since we expect per-particle detection efficiencies to be only mildly different across different channels, we simply use the same detection efficiencies found for the decaying-meson channel (A2) for the remaining background channels (A3) and (A4).

For a simple veto required to suppress the background, only a single track or calorimeter energy deposit is sufficient to reject a background process. For charged particles with  $\eta < 3.7$ , the tracking detectors will be able to reconstruct a particle trajectory, with additional information from calorimeter energy deposits also present, and extending beyond the tracker acceptance to  $\eta < 4.0$ . This makes vetoing straightforward because multiple detector subsystems will record relevant information used for the veto. For photons, only energy deposits in the electromagnetic calorimeters will be useful for vetoing. However, given the large number of radiation lengths present, the efficiency is still expected to be high.

From the simulation, we adopt the following single particle detection efficiencies for particles in the fiducial acceptance (in order from highest to lowest efficiency, based on ePIC detector instrumentation in the fiducial single-particle acceptance): i)  $\epsilon_\gamma \sim 99.8\%$  ii)  $\epsilon_{e^\pm} \sim 99.8\%$ , iii)  $\epsilon_{h^\pm} \sim 99.5\%$  for charged hadrons  $h$ , and iv)  $\epsilon_{\mu^\pm} \sim 95\%$ . For non-muonic states, these numbers are much tighter than the ones considered in Ref. [68], where a 95% single particle efficiency was assumed in the main ePIC detector volume for a fully reconstructed photon. Indeed, for

our purposes, we do not require a full reconstruction of particle kinematics but just a simple veto. In the case of muons, we assume a more conservative efficiency given how many of the  $\mu^+\mu^-$  events are near the edge of the ePIC acceptance region of  $\eta < 4.0$ . In cases where only one muon is within that acceptance, and near the edge, we place a 100 MeV threshold cut on its energy deposit to decide if that muon would be seen by ePIC. This leads to a loss of efficiency  $\sim 1\%$ . This could be improved by tightening the meson production cut to be well-within the ePIC main detector acceptance (e.g., from  $\eta < 4.0$  to  $\eta < 3.7 - 3.8$ ).

The resulting vetoing inefficiencies are  $\epsilon_{\text{ineff}}^{\gamma} = 2 \times 10^{-3}$  for bremsstrahlung producing a photon,  $\epsilon_{\text{ineff}}^{\gamma\gamma} = \epsilon_{\text{ineff}}^{e^+e^-} = 4 \times 10^{-6}$  for decays into two photons or into the electron-positron pair,  $2.5 \times 10^{-5}$  into charged hadrons, and  $2.5 \times 10^{-3}$  for the muons. Using the reported efficiencies, we present the residual background yields from the events (A3)-(A5) in Tbl. S1.

The veto performance could be further improved by combining multiple detector subsystems for signals from the decay products; using only fast simulation here makes our estimate conservative in terms of using a very low threshold for muon detection, but optimistic in not including other sources of background (e.g., machine backgrounds) or other sources of potential contamination. This can be improved by a future full simulation study with a finalized ePIC geometry, more mature reconstruction algorithms, and by simulating other potential backgrounds in that full simulation framework. In addition, for the muons, rejection power would potentially benefit from installing a dedicated muon detector system. Such a modification is an attractive option for the second detector at the EIC [63].

### 3. Instrumental and reconstruction effects

The last category is instrumental sources. They can mimic the exclusive missing-energy topology even in the absence of genuine invisible states. Below, we discuss the potential origins of such backgrounds and sketch the strategies that could mitigate them; a more quantitative discussion would require a full detector simulation, which is beyond the scope of this work.

Three categories are relevant:

(1) *Accidental overlaps and beam-related activity.* Beam-gas and beam-halo interactions may produce in-time signals in forward proton detectors uncorrelated with the hard interaction. A coincident off-momentum proton can be falsely associated with a genuine  $e + p \rightarrow e + X$  scattering lacking a leading proton, fabricating an exclusive  $e + p \rightarrow e' + p'$  candidate with apparent missing energy. Likewise, elastic  $e + p \rightarrow e' + p'$  events can be misclassified as missing energy events if unrelated neutral energy deposits (from beam losses or beam-gas interactions) compromise the forward veto logic.

These classes are suppressed by requiring tight bunch-crossing timing for the final-state proton and electron; consistency of the measured  $\xi = E_{p'}/E_p$  and  $Q^2$  with proton transport from the reconstructed vertex; and the absence of any extra detector activity above low thresholds in central and forward calorimetry and tracking.

(2) *Material interactions and local inefficiencies.* Photons emitted at small polar angles may convert upstream in windows or beam pipe components, with secondaries steered out of instrumented acceptance by magnetic elements. Tight collimation of photons from  $P = \{\pi^0, \eta, \eta'\}$  decays at high energy,  $\Delta\theta_{\gamma\gamma} \sim 2m_P/E_P$ , increases the probability that both photons traverse mechanical gaps or non-instrumented apertures. In these configurations, the net transverse momentum carried by the undetected neutral system is typically negligible, recovering the elastic-balance pattern  $|\mathbf{p}_{T,e'}| \simeq |\mathbf{p}_{T,p'}|$  despite hadronic emission. We mitigate these reducible backgrounds by imposing a global activity veto (including zero-degree and very-forward detectors), a narrow rejection band around  $|\mathbf{p}_{T,e'}| \approx |\mathbf{p}_{T,p'}|$ , and stability checks versus azimuth and pseudorapidity that expose crack-induced clustering. Events violating any of these criteria are rejected.

(3) *Reconstruction tails and calibration biases.* Possible background sources of this type include: small angular biases at very forward electrons alter  $Q^2 = |t_e|$  and the transverse-momentum correlation, allowing elastic radiative events to evade elastic-balance rejections or, conversely, pushing signal-like events into vetoed regions; and cluster merging of collimated  $\gamma\gamma$  from  $\pi^0$  decays can also defeat photon identification and vetoes. It may be possible to control these effects by enforcing per-object pointing to the primary vertex, redundant timing for  $e$  and  $p$  consistent with the event time, cross-calibrated energy and angle scales (e.g., track-calorimeter consistency for  $e$ ), and kinematic self-consistency tests requiring  $M_X^2$  to be compatible with the measured  $(\xi, t_p)$  within resolution. For many final states, it is reasonable to expect near 100% vetoing efficiency, assuming they are within the  $\eta < 4.0$  acceptance of ePIC. For final states with muons, experiments rely on minimum-ionizing signals in the hadronic calorimeters. Given the depth of these HCALs in ePIC (all  $> 4$  hadronic interaction lengths), the muons will interact with the HCAL volumes, but a full analysis of muon detection with appropriate thresholds would be better-suited to understand the full efficiency. In general, tightening the meson pseudorapidity cut to  $\eta < 3.7 - 3.8$  to fully ensure that the daughters fall within the acceptance, and to ensure charged final states have both track and calorimeter information, would enhance the vetoing efficiency by reducing losses near fiducial acceptance boundaries.

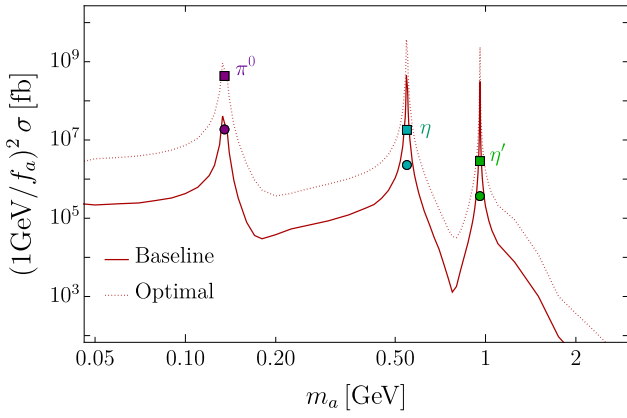


FIG. S1. The production cross section of the ALPs in the model of Eq. (3) with the reference choice  $f_a = 1$  GeV with the two setups from Tbl. I: Baseline (solid) and Optimal (dashed). We also show the  $\pi^0$  and  $\eta^{(\prime)}$  production cross sections for the Baseline (circle) and Optimal (square) selections.

#### 4. Comment on reconstructing invariant mass

An additional handle for background rejection for all three categories discussed above could, in principle, be obtained from reconstructing the invariant mass of the missing state  $m_{\text{inv},X}(p_{e'}, p_{p'})$ . Namely, when targeting the invisible decays of a specific meson  $P$ , it is possible to impose a requirement  $|m_{\text{inv},X} - m_P| < \delta$  to suppress contributions from other resonances and their visible decays. In practice, however, the missing mass resolution is highly sensitive to beam imperfections and to the kinematic smearing of  $p_{e'}$  and  $p_{p'}$ , so even modest distortions can broaden the  $m_{\text{inv},X}$  distribution to  $\mathcal{O}(100\%)$ , making this handle very challenging to exploit. In addition, the  $m_{\text{inv},X}$  reconstruction benefits only marginally from decreasing beam energy down to the minimal possible  $E_p = 41$  GeV and  $E_e = 5$  GeV, since the intrinsic difficulty of reconstructing missing mass with smeared collider kinematics persists even at lower energies.

#### Appendix B: EIC sensitivity estimation

In this section, we describe our calculation of the EIC sensitivity. We briefly discuss the impact of the selection criteria on the signal yield, as well as comment on the complications arising if considering the EIC setups with high-energy beam configuration. A more detailed discussion, including the investigation of the impact of various selection criteria on the signal yield, may be found in Ref. [60].

In Tbl. S2, we report the cross-section for each meson under Baseline and Optimal selection criteria from Tbl. I, before ( $\sigma_{\text{tot}}$ ) and after ( $\sigma_{\text{sel}}$ ) imposing selection criteria, while in Fig. S1, we also report the ALP post-selection production cross-section  $\sigma_{\text{sel}}$ . The selection ef-

ficiency (the ratio of  $\sigma_{\text{sel}}$  to the total production cross-section  $\sigma_{\text{tot}}$ ) is

$$\epsilon \equiv \frac{\sigma_{\text{sel}}}{\sigma_{\text{tot}}} \simeq \begin{cases} 0.005-0.009, & \text{Baseline} \\ 0.25, & \text{Optimal} \end{cases} . \quad (\text{B1})$$

This illustrates the large difference in selection efficiency arising from changes in the initial energies, on which the total cross section depends only mildly.

Using  $\sigma_{\text{sel}}$ , we estimate the EIC sensitivity:

$$\sum_{X=\pi^0, \eta, \eta'} \mathcal{L} \cdot \sigma_{\text{sel}} > \begin{cases} 3, & N_{\text{bg}} = 0 \\ 2\sqrt{N_{\text{bg}}}, & \text{otherwise} \end{cases} . \quad (\text{B2})$$

Finally, let us comment on the complexities of utilizing the MPE search for the EIC setups with high total  $ep$  energy. Increasing the energy shifts the kinematics of the  $X$  state to the partially instrumented domain  $\eta_X > 4$ , rendering the  $\eta_X < 4$  cut very harmful to the signal event yield. This problem may be mitigated by adding the partially instrumented  $4.5 < \eta_X < 6$  domain to the event selection. The price for this is a significantly increased vetoing inefficiency. A more detailed investigation of the inefficiencies for the  $4.5 < \eta < 6$  window requires full simulation. However, for illustrative purposes, we considered the configuration with the highest possible energy,  $E_p = 275$  GeV,  $E_e = 18$  GeV, and repeated the same fast simulation we conducted for the (100, 10) GeV configuration. Compared to the energy configuration of the Baseline setup, we found that the vetoing inefficiency increases to 2% for  $\rho^0 \rightarrow \pi^+ \pi^-$ , 4% for  $\phi \rightarrow K\bar{K}$ , 0.2% for  $\pi^0 \rightarrow e^+ e^-$ , and 5% for  $\pi^0 \rightarrow \gamma\gamma$ . The inefficiency may be reduced by increasing the instrumentation of the  $\eta_X > 4$  region. For the ePIC detector, this is very complicated for  $\eta_X > 4$  due to the lack of space for new detectors, but it may be possible for the possible second detector.

#### Appendix C: More on invisible signatures

In this section, we compare signatures with invisible decays arising in the models with hadronically coupled ALPs.

The generic Lagrangian reads

$$\mathcal{L}_a \supset -\frac{c_g \alpha_s}{8\pi} \frac{a}{f_a} G^{\mu\nu} \tilde{G}_{\mu\nu} + \frac{\partial_\mu a}{f_a} \bar{q} c_q \gamma^\mu \gamma_5 q - \bar{q} M_q e^{2i\gamma^5 \beta_q \frac{a}{f_a}} q + ig_{a\chi} a \bar{\chi} \gamma^5 \chi . \quad (\text{C1})$$

It includes not only gluonic coupling, but also couplings to quarks in the axial-vector current,  $c_q$ , and in the quark mass term,  $\beta_q$ . Additional couplings that do not contribute to the relevant processes have been omitted. The model presented in Eq. (3) is equivalent to taking  $c_g = -2$  and  $c_q = \beta_q = 0$ .

$P$	$\text{BR}(P \rightarrow \text{inv})_{\text{SM}}$	$\text{BR}(P \rightarrow \text{inv})_{\text{current}}$	Selection	$\sigma_{\text{tot}} [\text{fb}]$	$\sigma_{\text{sel}} [\text{fb}]$
$\pi^0$	$4 \times 10^{-23}$ [28]	$4.4 \times 10^{-9}$ [43]	Baseline	$4 \times 10^{11}$	$2 \times 10^7$
			Optimal	$3 \times 10^{11}$	$8 \times 10^{10}$
$\eta$	$1 \times 10^{-18}$ [28]	$1.1 \times 10^{-4}$ [44]	Baseline	$3 \times 10^8$	$2 \times 10^6$
			Optimal	$3 \times 10^8$	$7 \times 10^7$
$\eta'$	$5 \times 10^{-18}$ [28]	$2.1 \times 10^{-4}$ [44]	Baseline	$4 \times 10^7$	$4 \times 10^5$
			Optimal	$4 \times 10^7$	$1 \times 10^7$

TABLE S2. Pseudoscalar mesons  $P = \pi^0, \eta, \eta'$ , the branching ratios of their invisible decays as predicted in the SM, the current experimental bounds on their invisible decays coming from the NA64h search [44], as well as the event cross-section before ( $\sigma_{\text{tot}}$ ) and after ( $\sigma_{\text{sel}}$ ) imposing selection. We report here the results for the two sets of selection criteria from Tbl. I of the main text: Baseline and Optimal.

We define the following combinations of the ALP couplings:

$$\bar{c}_q \equiv c_q + \beta_q, \quad \bar{c}_g \equiv c_g + \langle \beta_q \rangle, \quad (\text{C2})$$

where  $\langle \dots \rangle = 2\text{Tr}(\dots)$ , with the trace being performed in flavor space. These combinations have the property of being invariant under an axial rotation of the quark, and thus measurable quantities may depend on them [123].

The two contributions to the invisible events in this model are: (i) decays of *on-shell ALPs*,  $a \rightarrow \text{inv}$ , and (ii) decays of pseudoscalar mesons  $P$  via *off-shell ALPs*,  $P \rightarrow a^* \rightarrow \text{inv}$ .

The calculation of the ALP production cross-section, which determines the sensitivity to the on-shell contribution, is discussed in detail in Ref. [60]; we refer to this work and do not provide details here. The branching ratio of invisible ALP decays reads

$$\text{BR}(a \rightarrow \text{inv}) = \frac{\Gamma(a \rightarrow \chi\bar{\chi})}{\Gamma(a \rightarrow \chi\bar{\chi}) + \Gamma(a \rightarrow \text{vis})}, \quad (\text{C3})$$

where  $\Gamma(a \rightarrow \chi\bar{\chi}) = g_{a\chi}^2 \sqrt{m_a^2 - 4m_\chi^2}/8\pi$  is the invisible width and  $\Gamma(a \rightarrow \text{vis}) \propto f_a^{-2}$  is the decay width into visible states originating from the coupling to hadrons (see Refs. [122, 123]). Parametrically, for allowed couplings  $f_a$ ,  $\text{BR}(a \rightarrow \text{inv})$  is very close to unity for  $g_{a\chi} \gtrsim 10^{-3}$  and even smaller, depending on the ALP mass.

Now, let us proceed to the off-shell contribution. Below, we calculate the branching ratios of the pseudoscalar mesons  $\pi^0$  and  $\eta^{(\prime)}$  into the invisible state  $\chi\bar{\chi}$  and then discuss the range of ALP masses and couplings probed by the two contributions.

Decays of pseudoscalar mesons via off-shell ALPs may be interpreted in terms of mixing between the ALPs and  $P$ . The relation between the interaction states and the mass states (labeled as 'phys') is given by

$$a = a_{\text{phys}} + \frac{f_\pi}{f_a} \sum_{P=\pi, \eta, \eta'} g_{aP} P_{\text{phys}}, \quad (\text{C4})$$

where  $f_\pi = 92$  MeV. The coefficients  $g_{aP}$  are calculated using the approach of Refs. [101, 122, 123]:

$$g_{a\pi} = \frac{m_\pi^2}{m_a^2 - m_\pi^2} \left\{ (\bar{c}_u - \bar{c}_d) + \frac{\delta_I}{4} \left[ -2\bar{c}_g + \frac{3m_\pi^2}{(m_\eta^2 - m_\pi^2)} \left( \bar{c}_u + \bar{c}_d - \frac{2}{3}\bar{c}_s \right) \right] \right\}, \quad (\text{C5})$$

$$g_{a\eta} = \frac{2}{\sqrt{6}} \frac{1}{m_a^2 - m_\eta^2} \left\{ m_\eta^2 \left( -\frac{\bar{c}_g}{2} + \bar{c}_u + \bar{c}_d - \bar{c}_s \right) + m_\pi^2 \frac{\bar{c}_g}{2} + \delta_I \frac{m_\pi^2 m_\eta^2}{m_\eta^2 - m_\pi^2} (\bar{c}_d - \bar{c}_u) \right\}, \quad (\text{C6})$$

$$g_{a\eta'} = \frac{4}{\sqrt{3}} \frac{1}{m_a^2 - m_{\eta'}^2} \left\{ \frac{m_\eta^2}{2} (-\bar{c}_g + 2\bar{c}_u + 2\bar{c}_d + 4\bar{c}_s) + \frac{m_\pi^2}{4} (2\bar{c}_g - 3\bar{c}_u - 3\bar{c}_d - 6\bar{c}_s) + \frac{\delta_I}{4} \frac{m_\pi^2 m_{\eta'}^2}{m_{\eta'}^2 - m_\pi^2} (\bar{c}_d - \bar{c}_u) \right\}, \quad (\text{C7})$$

where  $\delta_I \equiv (m_d - m_u)/(m_d + m_u)$  is the isospin-breaking parameter.

For the gluonic ALP model (Eq. (3)), these are:

$$g_{a\pi} = \delta_I \frac{m_\pi^2}{m_a^2 - m_\pi^2}, \quad (\text{C8})$$

$$g_{a\eta} = \frac{2}{\sqrt{6}} \frac{m_\eta^2 - m_\pi^2}{m_a^2 - m_\eta^2}, \quad (\text{C9})$$

$$g_{a\eta'} = \frac{4}{\sqrt{3}} \frac{m_\eta^2 - m_\pi^2}{m_a^2 - m_{\eta'}^2}. \quad (\text{C10})$$

The resulting branching ratio of the process  $P \rightarrow \bar{\chi}\chi$  via off-shell ALP is

$$\text{BR}(P \rightarrow \bar{\chi}\chi) = \frac{m_P}{8\pi\Gamma_P} \left( \frac{f_\pi}{f_a} g_{aP} g_{a\chi} \right)^2 \sqrt{1 - \frac{4m_\chi^2}{m_P^2}}, \quad (\text{C11})$$

where  $\Gamma_P$  is the total decay width of  $P$ .

As a consequence, we can recast the projected EIC sensitivity to invisible meson decays,  $[\text{BR}(P \rightarrow \text{inv})]_{\text{EIC}}$ , under the assumed background scenario, into a corresponding projected reach in the coupling combination  $g_{a\chi}/f_a$ :

$$\frac{g_{a\chi}}{f_a} > \frac{1}{f_\pi g_{aP}} \sqrt{\frac{8\pi\Gamma_P [\text{BR}(P \rightarrow \text{inv})]_{\text{EIC}}}{\sqrt{m_P^2 - 4m_\chi^2}}}. \quad (\text{C12})$$

For the case of the gluonic ALPs with  $c_g = -2$ ,  $\beta_q = c_q = 0$ , using Eqs. (C8)–(C12) for  $m_\chi = 0$  and  $m_a \gg m_P$ , we can derive the asymptotic form of the EIC reach:

$$m_a \sqrt{\frac{f_a/g_{a\chi}}{10^2 \text{ GeV}}} > 10 \left( \frac{2 \times 10^{-9}}{[\text{BR}(\pi^0 \rightarrow \text{inv})]_{\text{EIC}}} \right)^{1/4} \text{ GeV}, \quad (\text{C13})$$

$$m_a \sqrt{\frac{f_a/g_{a\chi}}{10^2 \text{ GeV}}} > 17 \left( \frac{1 \times 10^{-8}}{[\text{BR}(\eta \rightarrow \text{inv})]_{\text{EIC}}} \right)^{1/4} \text{ GeV}, \quad (\text{C14})$$

$$m_a \sqrt{\frac{f_a/g_{a\chi}}{10^2 \text{ GeV}}} > 6 \left( \frac{8 \times 10^{-8}}{[\text{BR}(\eta' \rightarrow \text{inv})]_{\text{EIC}}} \right)^{1/4} \text{ GeV}. \quad (\text{C15})$$

We learn that invisible meson decays at the EIC will be sensitive to ALPs with  $m_a \sim \mathcal{O}(10 \text{ GeV})$  for  $f_a/g_{a\chi} \sim 100 \text{ GeV}$ .

Next, we discuss the complementarity of the on-shell and off-shell ALP contributions to the MPE events. The yield of events with on-shell ALPs scales with  $\text{BR}(a \rightarrow \text{inv})/f_a^2$ , whereas the number of events with off-shell ALPs behaves as  $g_{a\chi}^2/f_a^2$ . As a result, they prefer different domains of the parameter space. In particular, given the behavior of  $\text{BR}(a \rightarrow \text{inv})$ , the on-shell contribution is the main one for small  $g_{a\chi} \ll 1$ . On the other hand, the off-shell events dominate for larger  $g_{a\chi}$ . We demonstrate the EIC sensitivity to these two cases in the plane  $g_{a\chi} - f_a^{-1}$  in Fig. S2.

#### Appendix D: Interpreting current bounds from invisible meson decays

We estimate the bounds on the gluonic ALP model of Eq. (C1) coming from existing measurements of invisible meson decays. The NA62 collaboration reported bounds on invisible decays of the  $\pi^0$  meson in Ref. [43] and the process  $K^+ \rightarrow \pi^+ + \text{inv}$  in Ref. [129]. In both cases, the missing-mass technique has been adopted, so these are independent analyses disentangling the off-shell and

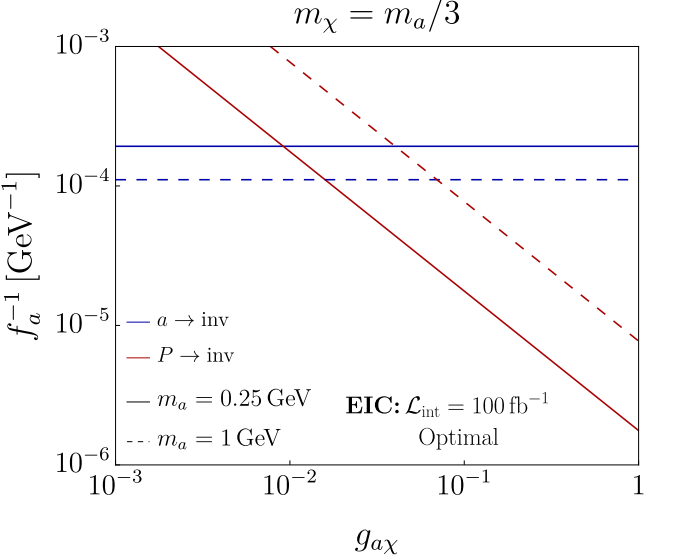


FIG. S2. Complementarity between two contributions to the missing-proton-energy events at the EIC: decays of pseudoscalar mesons (red) and of ALPs (blue), for two ALP masses  $m_a = 0.25 \text{ GeV}$  (solid) and  $1 \text{ GeV}$  (dashed), in the plane  $\{g_{a\chi}, f_a^{-1}\}$ . The curves show the lower bound of the sensitivity corresponding to the Baseline selection, under the assumption of zero background.

on-shell ALP decays. The resulting upper limit on the allowed branching ratio reads

$$[\text{BR}(\pi^0 \rightarrow \text{inv})]_{\text{NA62}} < 4.4 \times 10^{-9}, \quad (\text{D1})$$

$$[\text{BR}(K^+ \rightarrow \pi^+ + \text{inv})]_{\text{NA62}} \lesssim 2 \times 10^{-11}, \quad (\text{D2})$$

where the second bound is mass-dependent.

Within the model of Eq. (C1),  $\text{BR}(\pi^0 \rightarrow \bar{\chi}\chi)$  is given by Eq. (C11). The  $K \rightarrow \pi\chi\bar{\chi}$  rates can be written as

$$\text{BR}(K \rightarrow \pi\chi\bar{\chi}) = \text{BR}(K^+ \rightarrow \pi^+ a) \text{BR}(a \rightarrow \chi\bar{\chi}), \quad (\text{D3})$$

where  $\text{BR}(K^+ \rightarrow \pi^+ a)$  is given in Ref. [104] and  $\text{BR}(a \rightarrow \chi\bar{\chi})$  is Eq. (C3).

Next, we reinterpret the NA64h result, where a 50 GeV pion beam hits a fixed target. NA64h reported bounds on the invisible decay of particles produced in the process [44]

$$\pi^- + p \rightarrow n + \text{inv}. \quad (\text{D4})$$

The missing invariant mass was not reconstructed; therefore, the bound is imposed on the sum  $\sum_{X=\pi^0, \eta, \dots} N_X \cdot \text{BR}(X \rightarrow \text{inv})$ . Under the assumption that solely  $\eta(\eta')$  meson dominates the invisible event yield, the bounds read

$$[\text{BR}(\eta \rightarrow \text{inv})]_{\text{NA64h}} = 1.1 \times 10^{-4}, \quad (\text{D5})$$

$$[\text{BR}(\eta' \rightarrow \text{inv})]_{\text{NA64h}} = 2.1 \times 10^{-4}. \quad (\text{D6})$$

In the context of our ALP model, Eq. (C1), the bounds from off-shell ALP production can be read as

$$\sum_{P=\eta, \eta'} \frac{\text{BR}(P \rightarrow \bar{\chi}\chi)}{[\text{BR}(P \rightarrow \text{inv})]_{\text{NA64h}}} < 1. \quad (\text{D7})$$

For the case when on-shell ALP decays dominate, we would need to know the event rate after imposing the selection, which is obviously ALP-mass-dependent. However, we estimate it by using two assumptions. *First*, we assume that the matrix element of the process (D4) with the production of  $P = \pi^0, \eta, \eta', a$  is dominated by the  $t$ -exchange of vector mesons  $V = \rho, \phi, \omega$  and their excitations. The contribution from individual  $V$ -exchange scales as  $G_V(t) \times g_{\pi VP} \times g_{Vpn}$ , with  $G_V$  being reggeized propagator,  $g_{\pi VP}$  the  $\pi^- V^+ P$  constant, and  $g_{Vpn}$  the  $V^- pn$  constant (see Ref. [60]). Within the universal Regge-parameterization of the cross-section from [144] utilized in the NA64h analysis, it allows us to assume

$$\sigma_{\text{tot}}(\pi + p \rightarrow P + n) \propto \left| \sum_V g_{\pi VP} g_{Vpn} \right|^2, \quad (\text{D8})$$

for the total cross-section before imposing analysis-driven selection. Second, Ref. [44] mentions that the characteristic signal shape for  $\eta, \eta'$  events would be very similar. Therefore, for a good approximation, the selections are independent of  $P$  (or  $m_a$ ).

Following the above arguments, we estimate the NA64h bound on invisibly decaying ALPs in the following way:

$$\frac{N_{a \rightarrow \text{inv}}}{[N_{\eta' \rightarrow \text{inv}}]_{\text{NA64h}}} = \frac{\sigma_{\text{tot}}(\pi + p \rightarrow a + n)}{\sigma_{\text{tot}}(\pi + p \rightarrow \eta' + n)} \frac{\text{BR}(a \rightarrow \text{inv})}{[\text{BR}(\eta' \rightarrow \text{inv})]_{\text{NA64h}}} \lesssim 1. \quad (\text{D9})$$

where  $N_{a \rightarrow \text{inv}}$  is the number of invisible ALP decays within the NA64h selection, while  $[N_{\eta' \rightarrow \text{inv}}]_{\text{NA64h}}$  is the maximally allowed number of invisibly decaying  $\eta'$ , which is given by Eq. (D6). The ratio of the cross-sections is given by Eq. (D8), where the coupling  $g_{\pi Va} \propto f_a^{-1}$ . We have found that the bound does not exceed the  $B \rightarrow K + \text{inv}$  and  $K \rightarrow \pi + \text{inv}$  bounds except for the narrow vicinities of the  $\eta, \eta'$  masses; therefore, we neglect it. Accurate calculations of this bound and the NA64 sensitivity are left for future work.